Dragon Fruit Peel-Derived Heterogeneous Catalyst for Michael Addition Reactions and Methanolysis of PET Waste: A Green and Dual-Functional Approach

Vanlalngaihawma Khiangte,[a,b,1] Samson Lalhmangaihzuala,[a,1] ZT Laldinpuii,[a,b] Khiangte Vanlaldinpuia[a*]

[a]Department of Chemistry, Pachhunga University College, Mizoram University, Aizawl, 796001, Mizoram, India.

[b]Department of Chemistry, Mizoram University, Aizawl, Mizoram, 796001, India.

*Corresponding authors: mapuiakhiangte@pucollege.edu.in

[1]Equal contributions for the first two authors.

Characterization of DFPA Catalyst (Provided for Reference Only)

Since the DFPA catalyst was not freshly synthesized for this study, no additional characterization was conducted.[1] For reference, the previously reported characterization data are briefly summarized, and Temperature Programmed Desorption (NH_3 and CO_2 TPD) analysis was added additionally. As illustrated in **Table S1**, XRF results confirm potassium oxide (59.02%) as the predominant component, followed by MgO, CaO, and SiO_2 in varying concentrations. The excellent catalytic performance is attributed to the presence of these basic metal oxides, which act as active sites, and the synergistic effect of the mixed oxides.[2]

Table S1: XRF analysis of DFPA result.

Sl. No.	Chemical Component	Mass %
1.	K_2O	59.02
2.	MgO	5.71
3.	NiO	4.86
4.	CaO	3.18
5.	SiO_2	2.41
6.	Cr_2O_3	0.10
7.	Al_2O_3	0.04
8.	MnO	0.03

FT-IR spectra (see Figure S1a) show characteristic carbonate vibrations (1365, 1041, 879 cm^{-1}), metal–oxygen stretches (771, 702 cm^{-1}), M–O–K vibration (2167 cm^{-1}), and CO_2 adsorption band (2360 cm^{-1}), consistent with our previous findings.[3–5] Nitrogen adsorption–desorption analysis (**see Figure S1b**) of the catalyst exhibits a type IV isotherm with an H3-type hysteresis loop, characteristic of mesoporous materials.[6] The isotherm reveals monolayer adsorption at low relative pressure (P/P^o), followed by multilayer adsorption at intermediate pressures and capillary condensation at higher P/P^o, as indicated by the desorption hysteresis.[6,7] Pore size distribution as shown in **Figure S1c**, determined using the Barrett-Joyner-Halenda (BJH) method, ranged from 3.09 to 24.57 nm, with an average pore diameter

of 3.450 nm. The BET surface area and total pore volume were found to be 1.290 m^2/g and 0.004 cm^3/g, respectively. These mesoporous characteristics and moderate surface area are considered essential for catalysis. Distinct diffraction peaks observed in the XRD pattern of DFPA correspond to K_2O (JCPDS Nos. 77-2176, 77-2151) and K_2CO_3 (JCPDS No. 71-1466) at 2θ = 25.382°, 27.952°, 29.465°, 32.092°, 37.975°, 39.041°, 41.148°, 45.468°, and 57.561° (see Figure S1d). Additional peaks were assigned to CaO (JCPDS No. 82-1691), $CaCO_3$ (JCPDS No. 87-1863), and MgO (JCPDS No. 65-0476) at 2θ = 30.328°, 32.300°, 37.057°, 43.196°, and 54.395°. Minor crystalline phases, including SiO_2 (JCPDS No. 89-8949), Cr_2O_3 (JCPDS No. 84-0315), $NiCO_3$ (JCPDS No. 78-0210), and KCl (JCPDS No. 89-3619), were also detected at 2θ = 26.009°, 28.338°, 33.156°, 33.878°, 40.502°, 50.144°, and 58.665°.

Thermogravimetric analysis (**see Figure S2a**) demonstrated the thermal stability of DFPA, with an initial weight loss (7–13%) between 100–200 °C due to moisture evaporation, followed by decomposition of carbonates at higher temperatures. EDX analysis (as shown in Figure S2b) further confirmed the elemental composition, showing the presence of K (42.36%), O (39.46%), Ca (7.98%), Mg (4.30%), Cl (3.76%), P (1.31%), C (0.60%), and S (0.25%). Morphological analysis using SEM and TEM images (**see Figure S3**) revealed a rough, spongy surface morphology with abundant pores, supporting the mesoporous nature of DFPA. The particle sizes were estimated to range from 4–20 nm. As seen in **Figure S4**, XPS analysis confirmed the presence of Mg, Na, O, Ca, K, and C on the DFPA surface. The C 1s spectrum showed peaks at 284.84 eV and 288.94 eV, corresponding to C–C and C=O of carbonates.[2] The O1s peak at 530.86 eV indicated metal oxides,[3] while the K2p peaks at 295.08 eV and 292.44 eV confirmed K_2O and K_2CO_3.[8] Peaks at 346.61 eV, 350.52 eV (Ca2p), and 1303.94 eV (Mg1s) were assigned to CaO, $CaCO_3$, and MgO,[9] respectively. These results support the mixed metal oxide and carbonate composition revealed by XRD, XRF, and FT-IR analyses.

Temperature programmed desorption analysis using CO_2 and NH_3 confirms the presence of basic and acidic sites on the catalyst, as shown in **Figure S4g**. CO_2-TPD profile exhibited three desorption peaks at 148.4 ℃, 207.5 ℃, and 441.6 ℃, corresponding to weak, moderate, and strong basic sites, respectively. Meanwhile, the presence of weak and strong acidic sites was also confirmed as their corresponding peaks were observed at 206.5 ℃ and 450 ℃ in the NH_3-TPD profile. However, as evident from the profiles, the basic character predominates over the acidic nature, with the quantified basicity (0.462 mmol g^{-1}) exceeding the total acidity (0.393 mmol g^{-1}).

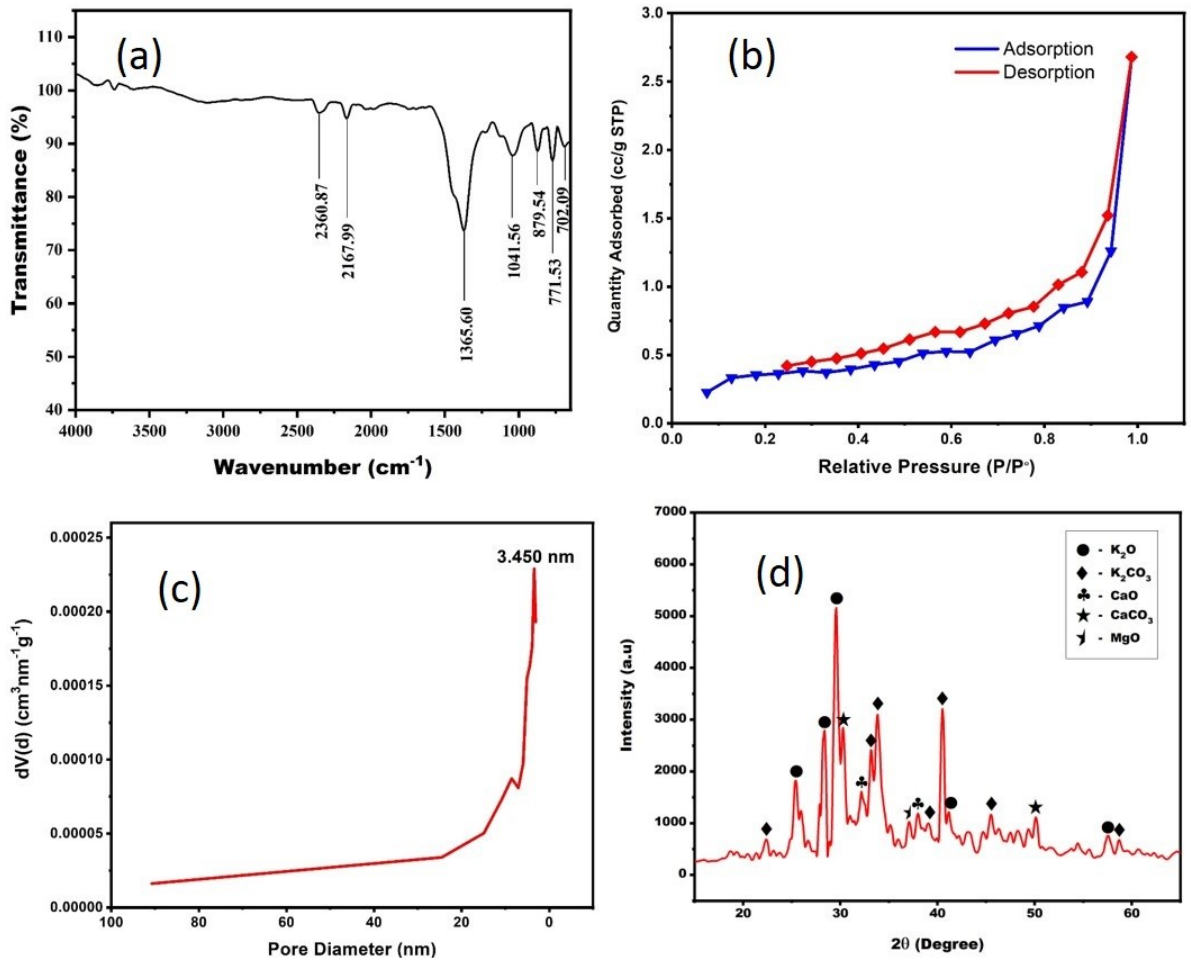

Figure S1: (a) FT-IR spectrum of DFPA; (b) N_2 adsorption-desorption isotherm of DFPA; (c) DFPA pore size distribution; (d) XRD data of DFPA.

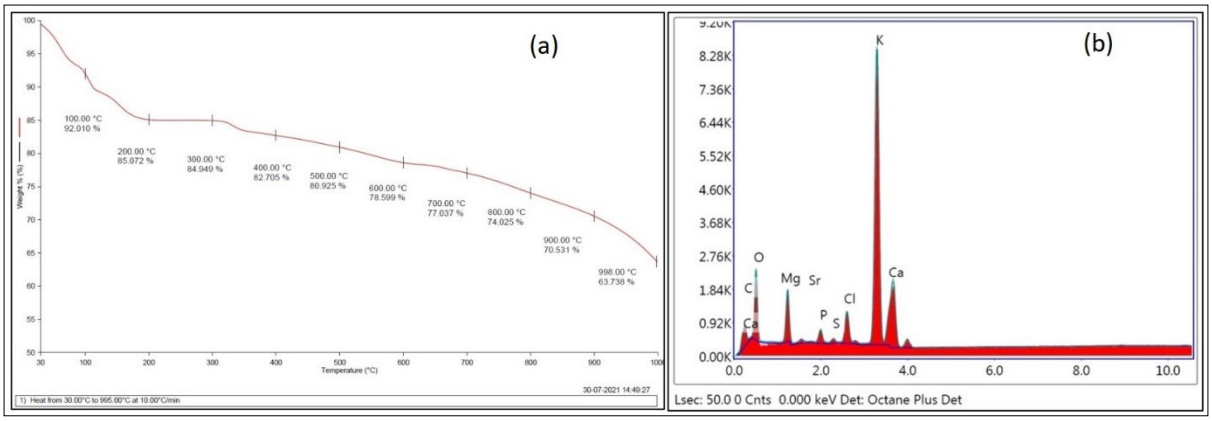

Figure S2: (a) TGA data of DFPA; (b) EDX spectra of DFPA

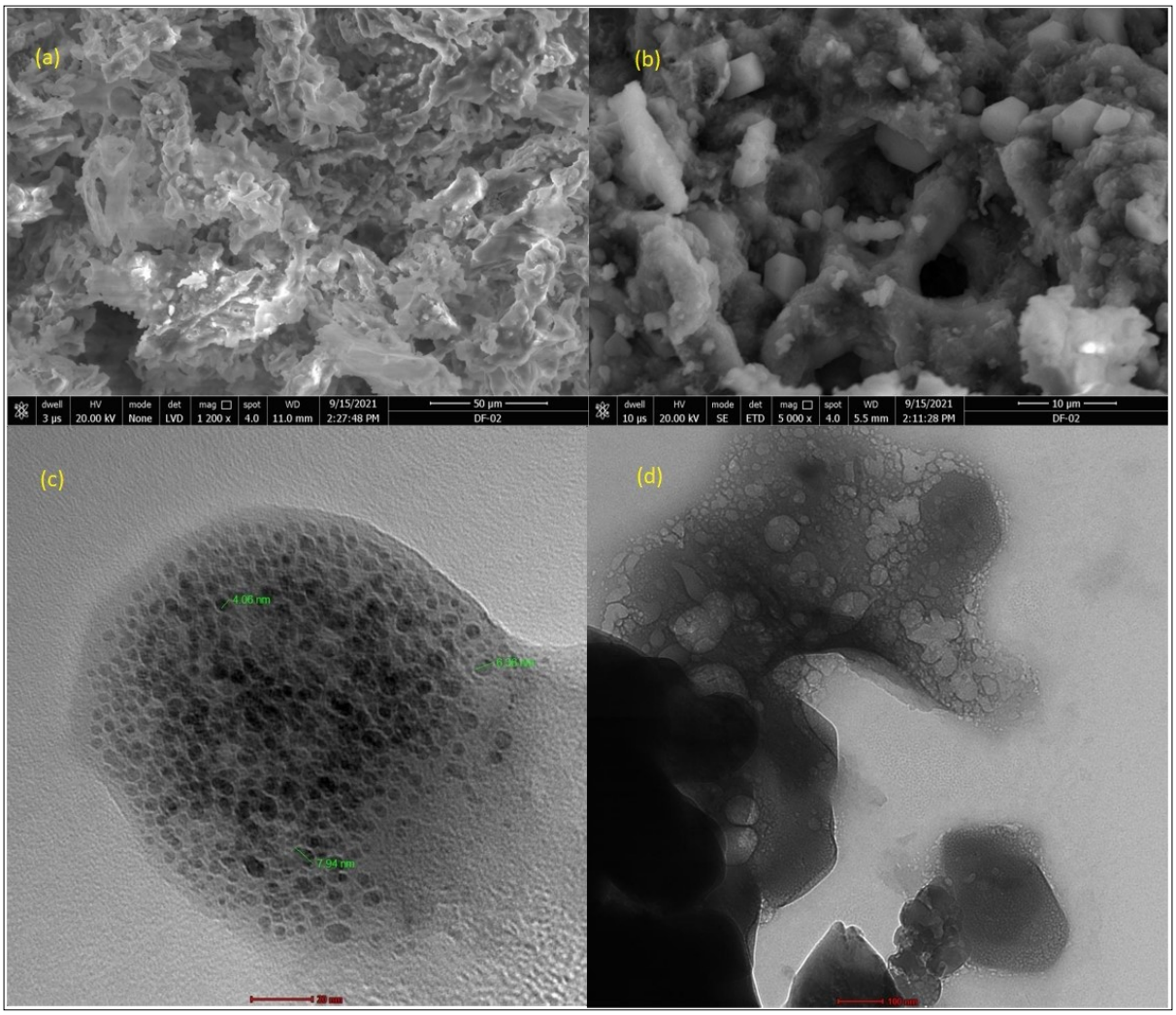

Figure S3: (a) and (b) SEM scanning of DFPA; (c) and (d) TEM scanning of DFPA

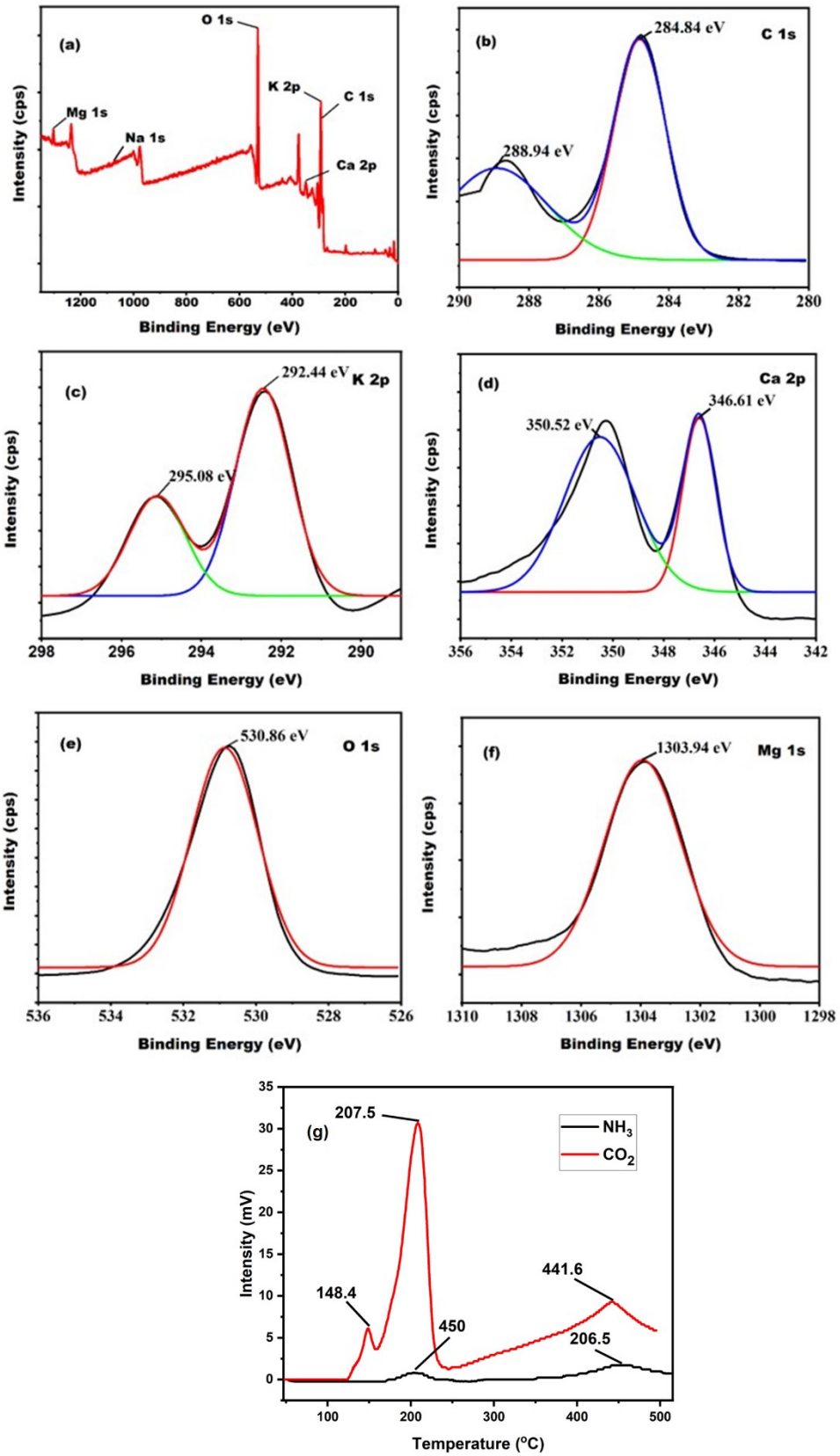

Figure S4: (a) XPS Full survey spectrum, (b) C 1s spectra, (c) K 2p spectra, (d) Ca 2p spectra, (e) O 1s spectra, (f) Mg 1s spectra, and (g) Temperature programmed desorption (NH_3 and CO_2).

Pressure Calculation using NIST Antoine equation[10,11]

$$log_{10} P = A - \frac{B}{T + C}$$

Where P is Pressure in bar, T is absolute Temperature (477.15 K), and A, B, and C are specific constants, and their corresponding value is given by NIST.[12] For methanol in the range 353-512 K, A = 5.15853, B = 1569.613, and C = -34.846. Thus, P = 40.72 bar = 4.072 Mpa.

NMR data of Michael adducts:

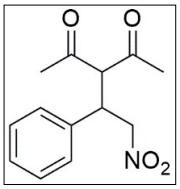

(3-(2-nitro-1-phenylethyl)pentane-2,4-dione, 3aa): ^{1}H NMR (400 MHz, $CDCl_3$): δ 7.38-7.10 (m, 5H), 4.60-4.52 (m, 2H), 4.31-4.14 (m, 2H), 2.20 (s, 3H), 1.86 (s, 3H) ppm. ^{13}C NMR (100 MHz, $CDCl_3$): δ 201.84, 201.13, 136.02, 129.33, 128.55, 127.96, 78.18, 42.81, 30.46, 29.63 ppm.

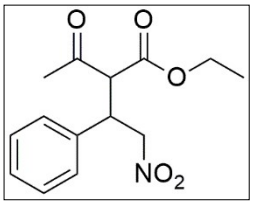

(Ethyl 2-acetyl-4-nitro-3-phenylbutanoate, 3ba): ^{1}H NMR (400 MHz, $CDCl_3$): δ 7.32-7.19 (m, 5H), 4.85-4.74 (m, 2H), 4.26-4.17 (m, 1H), 4.12 (d, 0.87H, *J* = 8 Hz), 4.03 (d, 0.22H, J = 8 Hz), 3.96 (q, 1H, *J* = 8 Hz), 2.30-2.05 (s, 3H), 1.27 (t, 0.71H, *J* = 8 Hz), 1.00 (t, 2.72H, *J* = 8 Hz) ppm. ^{13}C NMR (100 MHz, $CDCl_3$): δ 201.18, 200.37, 167.55, 166.88, 136.45, 129.41, 129.17, 128.95, 128.37, 128.29, 128.00, 127.92, 77.90, 77.80, 62.23, 62.00, 61.97, 61.69, 42.57, 42.32, 30.30, 30.10, 13.99, 13.68 ppm.

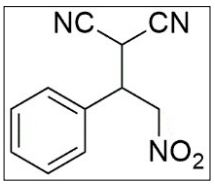

(2-(2-nitro-1-phenylethyl)malononitrile, 3ca): ^{1}H NMR (400 MHz, $CDCl_3$): δ 7.51-7.24 (m, 5H), 5.01-4.88 (m, 2H), 4.45 (d, 1H, *J* = 8 Hz), 4.14-4.09 (m, 1H) ppm. ^{13}C NMR (100 MHz, $CDCl_3$): δ 132.08, 130.30, 129.87, 127.82, 110.87, 110.76, 75.08, 43.47, 27.61 ppm.

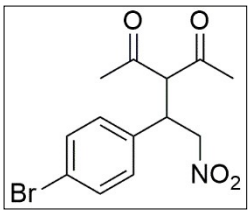

(3-(1-(4-bromophenyl)-2-nitroethyl)pentane-2,4-dione, 3ab): ^{1}H NMR (400 MHz, $CDCl_3$): δ 7.41 (d, 2H, *J* = 8 Hz), 7.04 (d, 2H, *J* = 8 Hz), 4.55 (d, 2H, *J* = 8 Hz), 4.27 (d, 1H, *J* = 8 Hz), 4.17-4.12 (m, 1H), 2.23 (s, 3H), 1.92 (s, 3H) ppm. ^{13}C NMR (100 MHz, $CDCl_3$): δ 201.44, 200.67, 135.15, 132.52, 129.68, 122.67, 77.85, 70.41, 42.23, 30.48, 29.76 ppm.

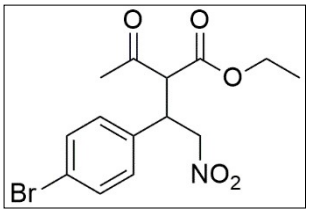

(Ethyl 2-acetyl-3-(4-bromophenyl)-4-nitrobutanoate, 3bb): ^{1}H NMR (400 MHz, $CDCl_3$): δ 7.44-7.07 (m, 4H), 4.85-4.66 (m, 2H), 4.24-4.13 (m, 2H), 4.10-4.05 (m, 1H), 4.00-3.94 (m, 1H), 2.28-2.07 (s, 3H), 1.26 (t, 1.56H, *J* = 4 Hz), 1.03 (t, 1.58H, *J* = 4 Hz) ppm. ^{13}C NMR (100 MHz, $CDCl_3$): δ 200.85, 200.03, 167.30, 166.67, 135.60, 135.57, 132.31, 132.11, 129.77, 129.67, 122.41, 122.35, 77.62, 77.46, 62.40, 62.18, 61.71, 61.49, 41.91, 41.74, 30.33, 30.06, 13.99, 13.75 ppm.

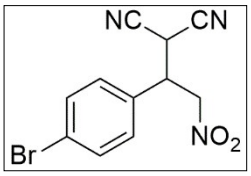

(2-(1-(4-bromophenyl)-2-nitroethyl)malononitrile, 3cb): ^{1}H NMR (400 MHz, $CDCl_3$): δ 7.27-7.13 (m, 4H), 4.82-4.72 (m, 2H), 4.45 (d, 1H, *J* = 8 Hz), 4.34-4.27 (m, 1H) ppm. ^{13}C NMR (100 MHz, $CDCl_3$): δ 133.43, 132.82, 129.11, 123.32, 110.48, 110.37, 76.45, 41.22, 27.41 ppm.

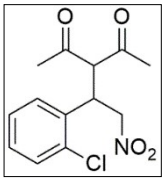

(3-(1-(2-chlorophenyl)-2-nitroethyl)pentane-2,4-dione, 3ac): ^{1}H NMR (400 MHz, $CDCl_3$): δ 7.45-7.15 (m, 4H), 4.86-4.73 (m, 2H), 4.69-4.59 (m, 2H), 2.28 (s, 3H), 2.04 (s, 3H) ppm. ^{13}C NMR (100 MHz, $CDCl_3$): δ 201.91, 200.93, 133.78, 133.47, 130.65, 129.72, 129.01, 127.66, 76.21, 68.90, 38.88, 30.91, 28.64 ppm.

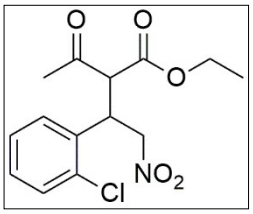

(Ethyl 2-acetyl-3-(2-chlorophenyl)-4-nitrobutanoate, 3bc): ^{1}H NMR (400 MHz, $CDCl_3$): δ 7.42-7.17 (m, 4H), 5.11-5.06 (m, 0.42H), 4.94-4.87 (m, 0.84H), 4.78-4.68 (m, 1H), 4.42 (d, 1H, *J* = 8 Hz), 4.25-4.18 (m, 1H), 4.05-3.97 (m, 1H), 2.33-2.21 (s, 3H), 1.26-1.01 (m, 3H) ppm. ^{13}C NMR (100 MHz, $CDCl_3$): δ 201.07, 200.34, 167.53, 166.64, 134.07, 134.00, 133.95, 133.86, 130.60, 130.43, 129.49, 129.42, 128.77, 128.63, 127.43, 127.31, 76.18, 75.57, 62.20, 62.10, 60.17, 60.09, 38.72, 30.42, 29.78, 13.97, 13.66 ppm.

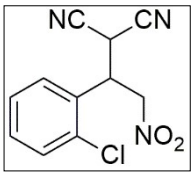

(2-(1-(2-chlorophenyl)-2-nitroethyl)malononitrile, 3cc): ^{1}H NMR (400 MHz, $CDCl_3$): δ 7.61-7.26 (m, 4H), 5.02-4.99 (m, 2H), 4.81-4.75 (m, 1H), 4.55 (d, 1H, *J* = 8 Hz) ppm. ^{13}C NMR (100 MHz, $CDCl_3$): δ 134.14, 131.41, 131.12, 129.54, 128.31, 127.76, 110.46, 110.14, 73.86, 39.75, 25.86 ppm.

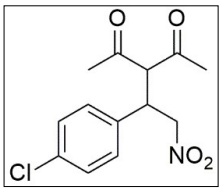

(3-(1-(4-chlorophenyl)-2-nitroethyl)pentane-2,4-dione, 3ad): R-4: ^{1}H NMR (400 MHz, $CDCl_3$): δ 7.39 (d, 2H, *J* = 8 Hz), 7.01 (d, 2H, *J* = 8 Hz), 4.54 (d, 1H, *J* = 8 Hz), 4.26 (d, 1H, *J* = 8 Hz), 4.17-4.13 (m, 1H), 2.21 (s, 3H), 1.90 (s, 3H) ppm. ^{13}C NMR (100 MHz, $CDCl_3$): δ 201.42, 200.65, 135.14, 132.51, 129.67, 122.65, 77.84, 70.40, 42.21, 30.48, 29.77 ppm.

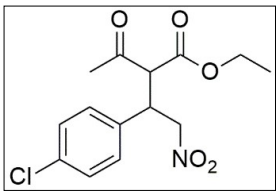

(Ethyl 2-acetyl-3-(4-chlorophenyl)-4-nitrobutanoate, 3bd): ^{1}H NMR (400 MHz, $CDCl_3$): δ 7.44 (d, 2H, *J* = 8 Hz), 7.10 (d, 2H, *J* = 8 Hz), 4.88-4.71 (m, 2H), 4.26-3.97 (m, 4H), 2.31 (s, 1.69H), 2.09 (s, 1.49H), 1.28 (t, 1.91H, *J* = 8 Hz), 1.05 (t, 1.36H, *J* = 8 Hz) ppm. ^{13}C NMR (100 MHz, $CDCl_3$): δ 200.83, 199.96, 167.28, 166.65, 135.53, 132.32, 132.13, 129.72, 129.63, 122.44, 122.37, 77.60, 77.44, 62.39, 62.17, 61.69, 61.50, 41.89, 41.73, 30.32, 30.07, 13.99, 13.67 ppm.

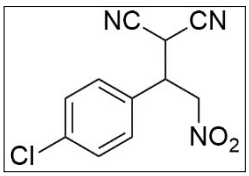

(2-(1-(4-chlorophenyl)-2-nitroethyl)malononitrile, 3cd): ^{1}H NMR (400 MHz, $CDCl_3$): δ 7.52 (d, 2H, *J* = 8 Hz), 7.12 (d, 2H, *J* = 8 Hz), 4.80-4.70 (m, 2H), 4.43 (d, *J* = 4 Hz), 4.33-4.26 (m, 1H) ppm. ^{13}C NMR (100 MHz, $CDCl_3$): δ 133.13, 132.85, 129.06, 123.37, 76.43, 41.25, 27.40 ppm.

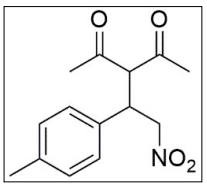

(3-(2-nitro-1-(p-tolyl)ethyl)pentane-2,4-dione, 3ae): ^{1}H NMR (400 MHz, $CDCl_3$): δ 7.13-7.06 (m, 4H), 4.61-4.20 (m, 4H), 2.30 (s, 3H), 2.28 (s, 3H), 1.94 (s, 3H) ppm. ^{13}C NMR (100 MHz, $CDCl_3$): δ 201.94, 201.22, 138.34, 132.85, 129.99, 127.80, 78.36, 70.78, 42.47, 30.42, 29.52, 21.05 ppm.

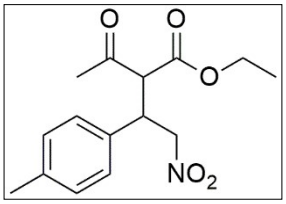

(Ethyl 2-acetyl-4-nitro-3-(p-tolyl)butanoate, 3be): ^{1}H NMR (400 MHz, $CDCl_3$): δ 7.12-7.06 (m, 4H), 4.85-4.71 (m, 2H), 4.25-3.94 (m, 4H), 2.29-2.03 (s, 6H), 1.27 (t, 1.60H, *J* = 4 Hz),

1.02 (t, 1.42H, J = 4 Hz) ppm. ^{13}C NMR (100 MHz, $CDCl_3$): δ 201.39, 200.62, 167.64, 166.98, 138.12, 137.99, 133.34, 133.24, 129.83, 129.60, 127.83, 127.77, 78.03, 62.19, 62.08, 61.94, 61.71, 42.31, 42.01, 30.31, 30.09, 21.04, 13.98, 13.69 ppm.

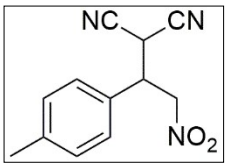

(2-(2-nitro-1-(p-tolyl)ethyl)malononitrile, 3ce): ^{1}H NMR (400 MHz, $CDCl_3$): δ 7.27-7.22 (m, 4H), 4.97-4.85 (m, 2H), 4.42 (d, 1H, J = 4 Hz), 4.30-4.24 (m, 1H), 2.37 (m, 3H) ppm. ^{13}C NMR (100 MHz, $CDCl_3$): δ 139.06, 130.25, 128.92, 127.25, 110.82, 110.69, 75.13, 41.48, 27.68, 21.21 ppm.

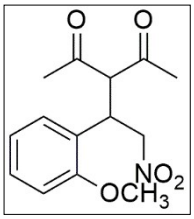

(3-(1-(2-methoxyphenyl)-2-nitroethyl)pentane-2,4-dione, 3af): ^{1}H NMR (400 MHz, $CDCl_3$): δ 7.28-6.86 (m, 4H), 4.81-4.76 (m, 1H), 4.61-4.56 (m, 2H), 4.50-4.45 (m, 1H), 3.87 (s, 3H), 2.25 (s, 3H), 1.93 (s, 3H) ppm. ^{13}C NMR (100 MHz, $CDCl_3$): δ 202.29, 201.68, 157.07, 130.29, 129.75, 123.55, 121.13, 111.28, 76.54, 68.83, 55.44, 39.09, 30.46, 28.94 ppm.

^{1}H and ^{13}C NMR spectra of Michael Addition Products

Figure S5: ^{1}H and ^{13}C NMR of **3aa** (3-(2-nitro-1-phenylethyl)pentane-2,4-dione).

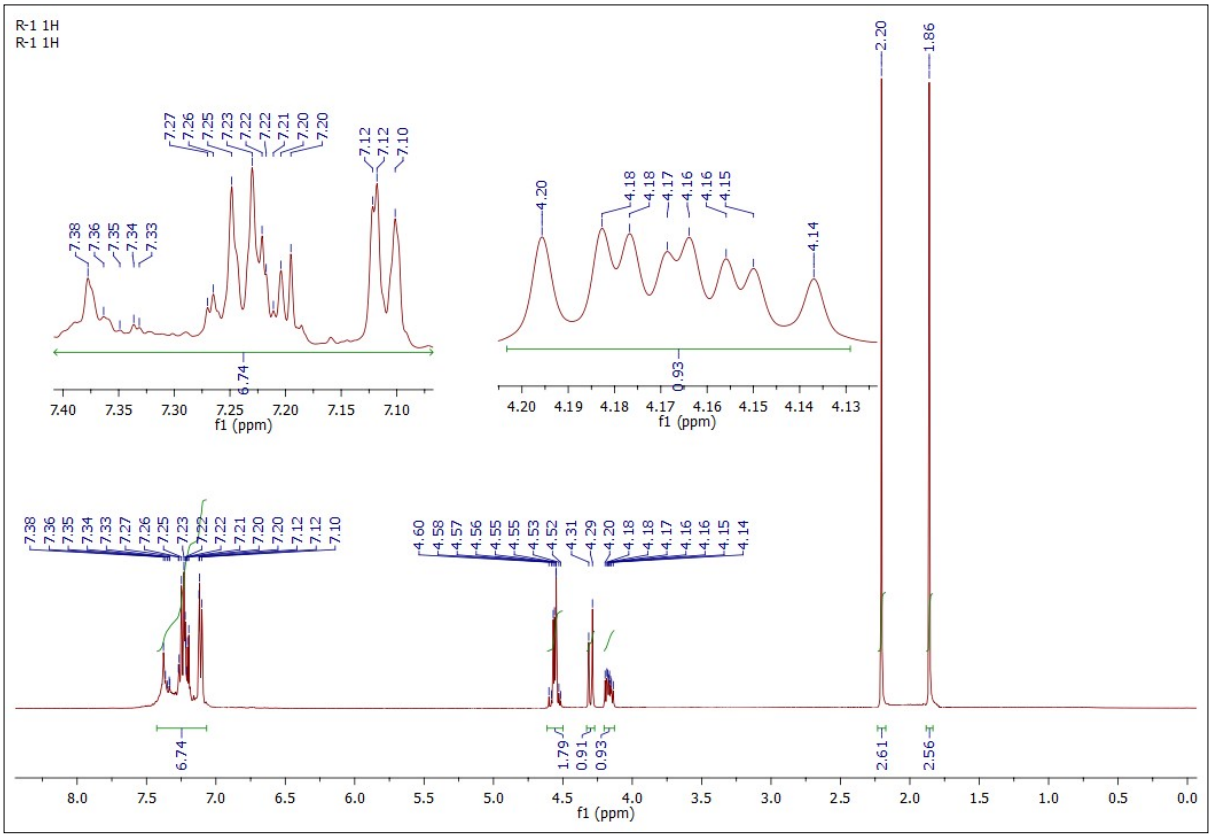

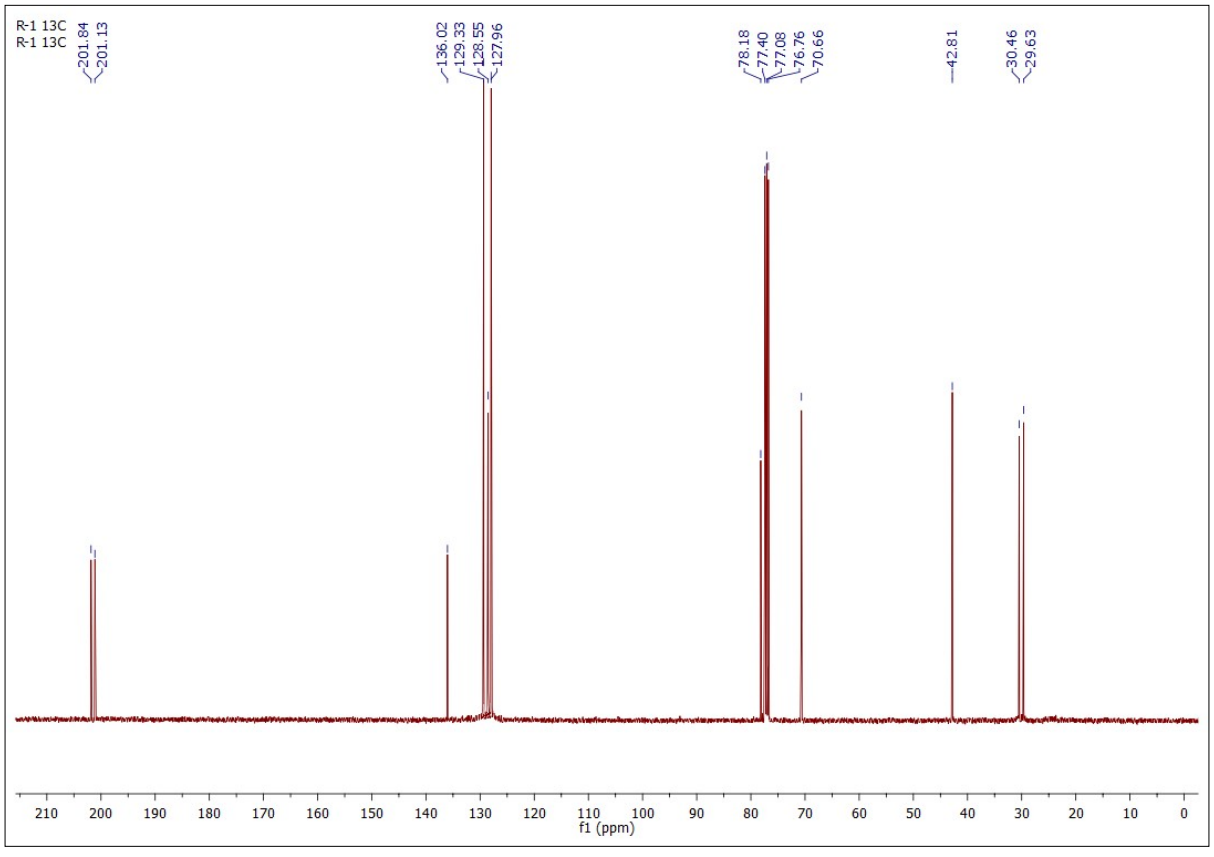

2-(CO)

Figure S6: ^{1}H and ^{13}C NMR of **3ba** (Ethyl 2-acetyl-4-nitro-3-phenylbutanoate).

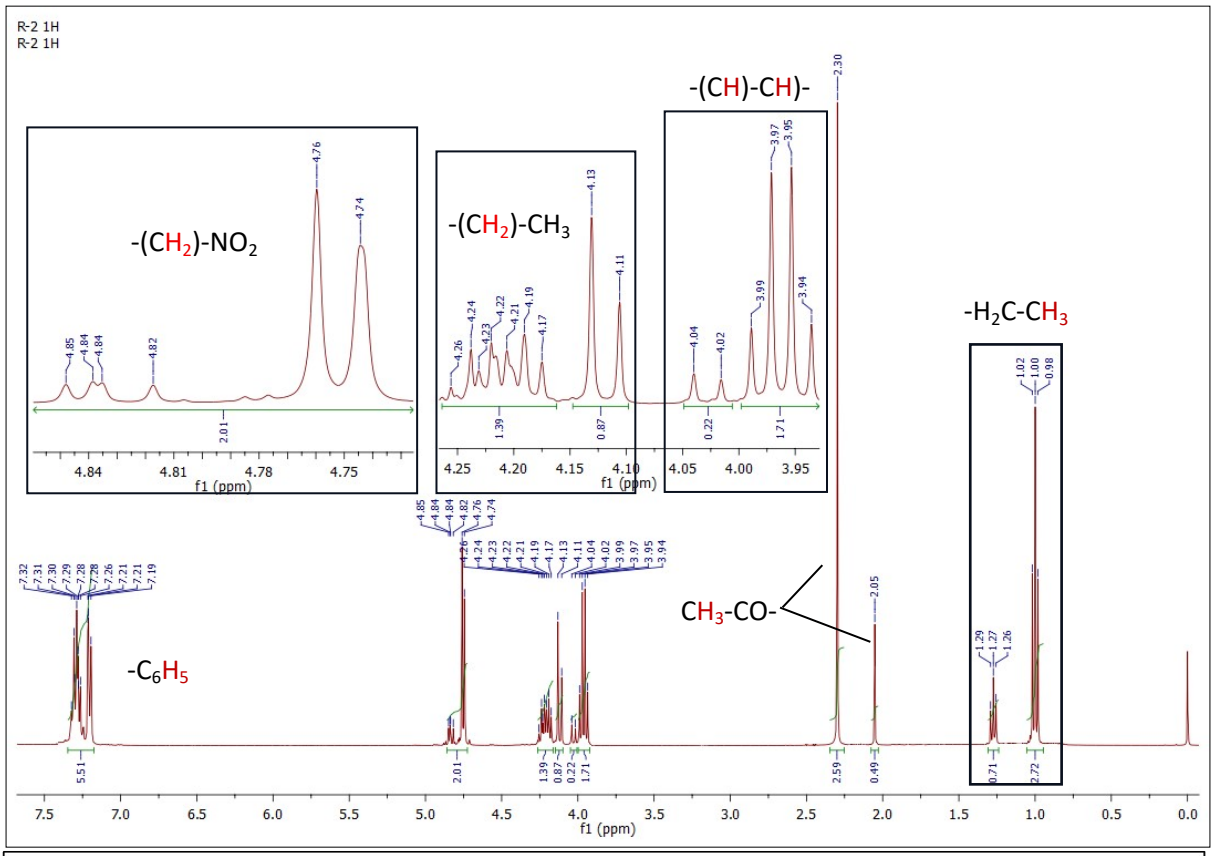

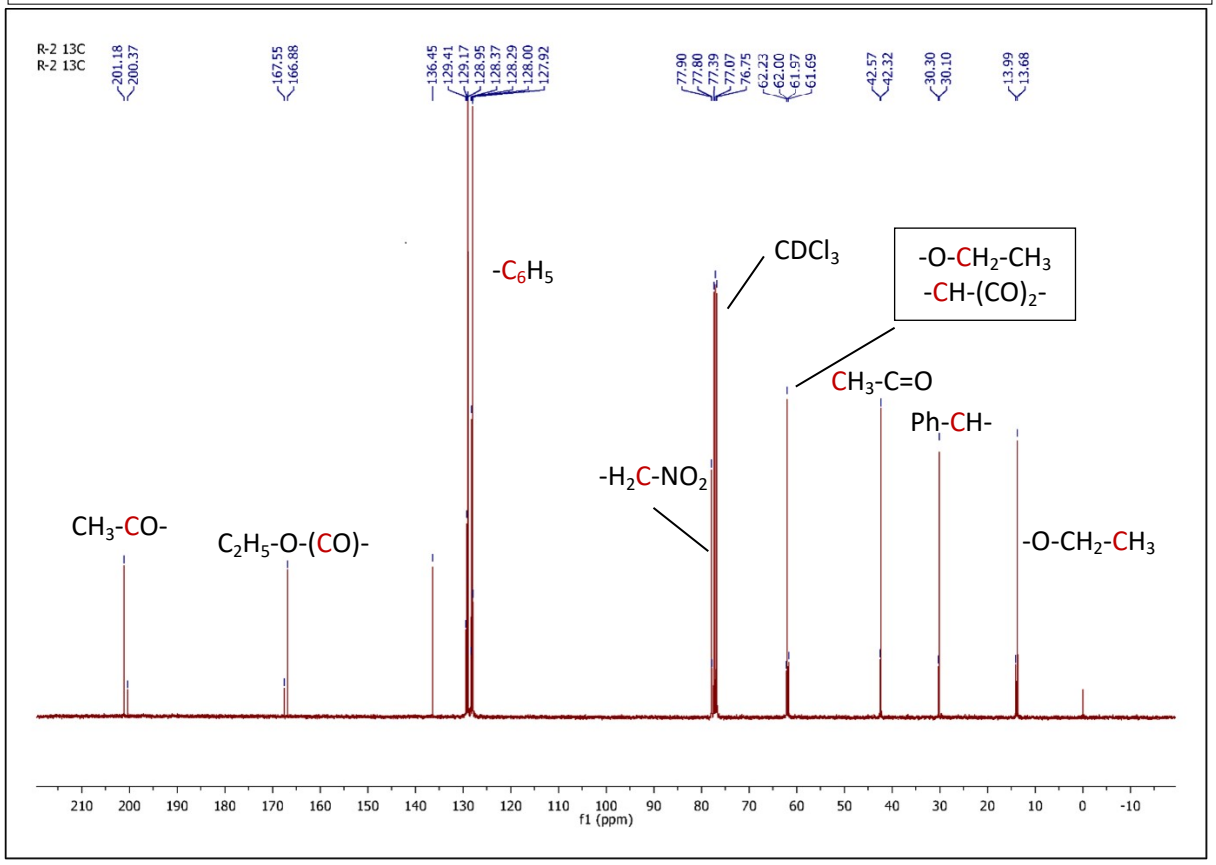

Figure S7: ^{1}H and ^{13}C NMR of **3ca** (2-(2-nitro-1-phenylethyl)malononitrile).

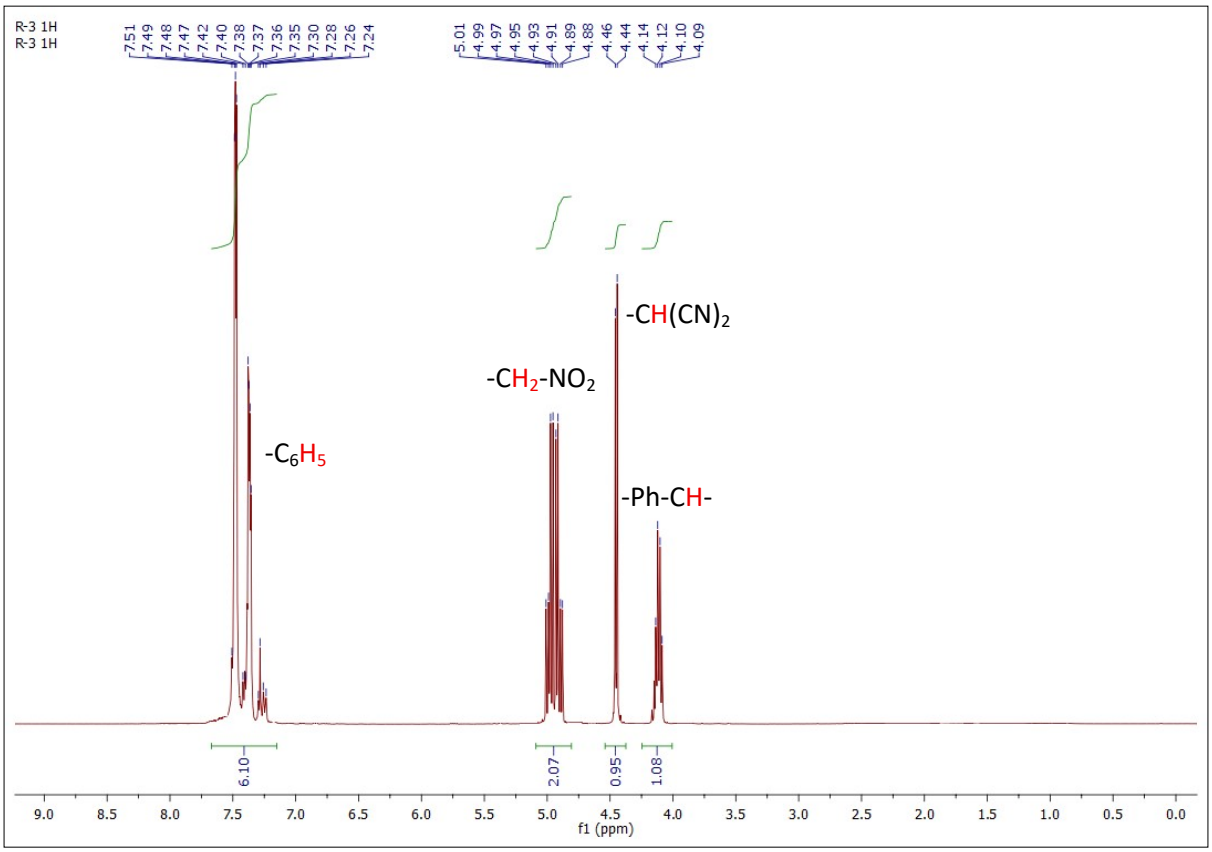

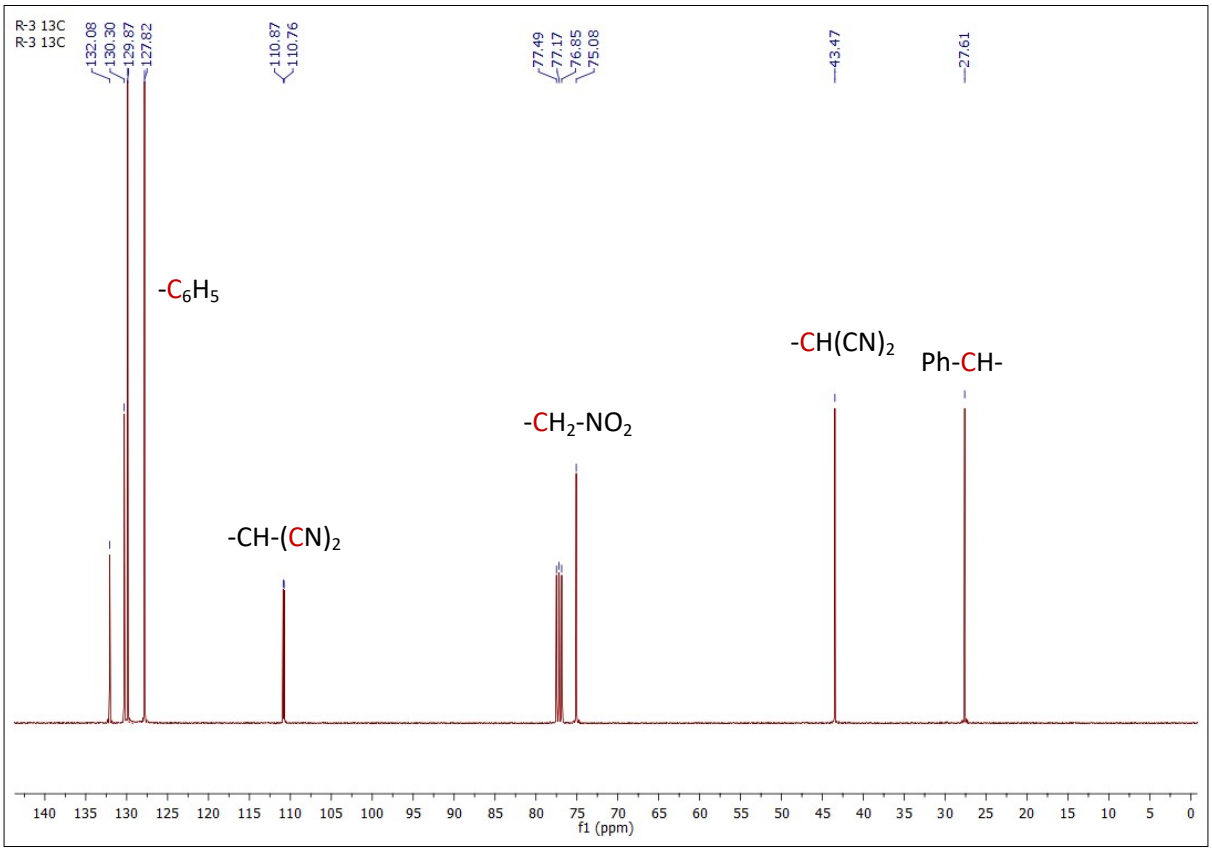

Figure S8: ^{1}H and ^{13}C NMR of **3ab** (3-(1-(4-bromophenyl)-2-nitroethyl)pentane-2,4-dione).

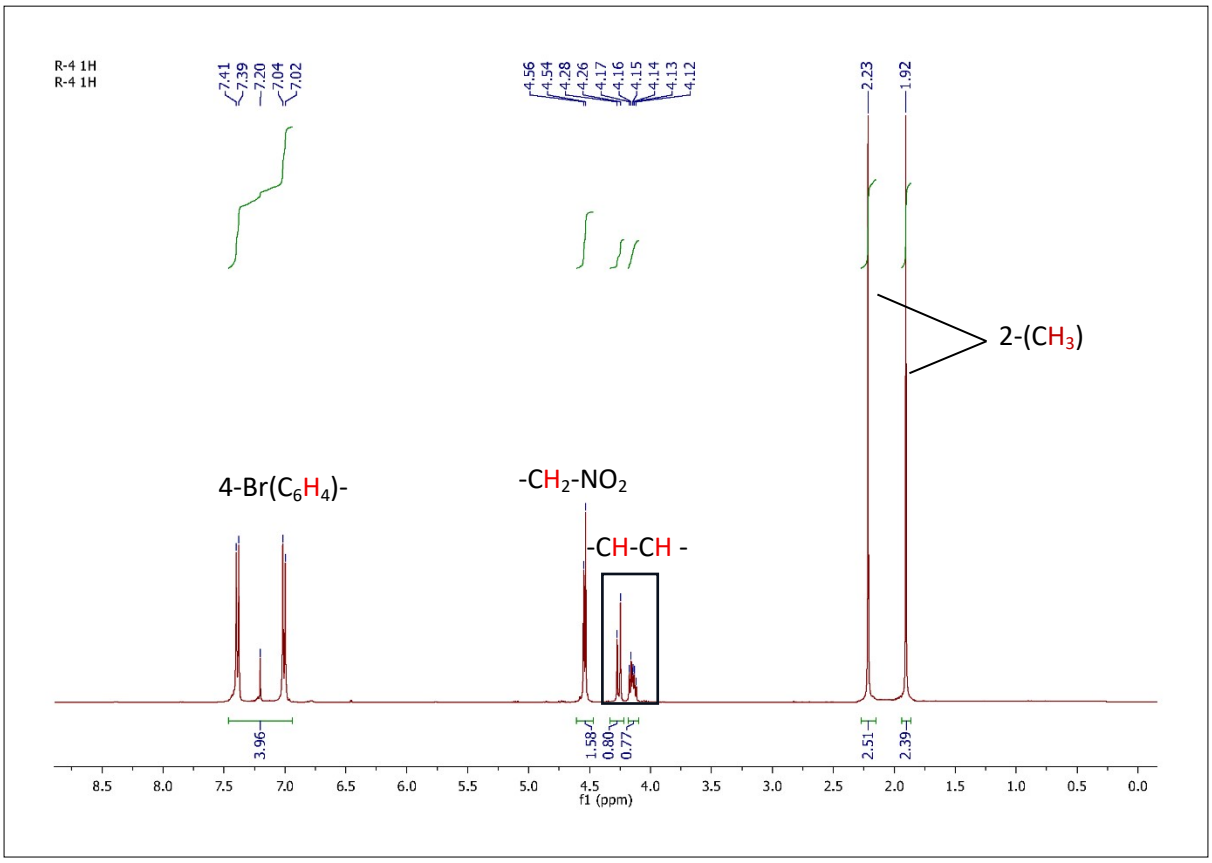

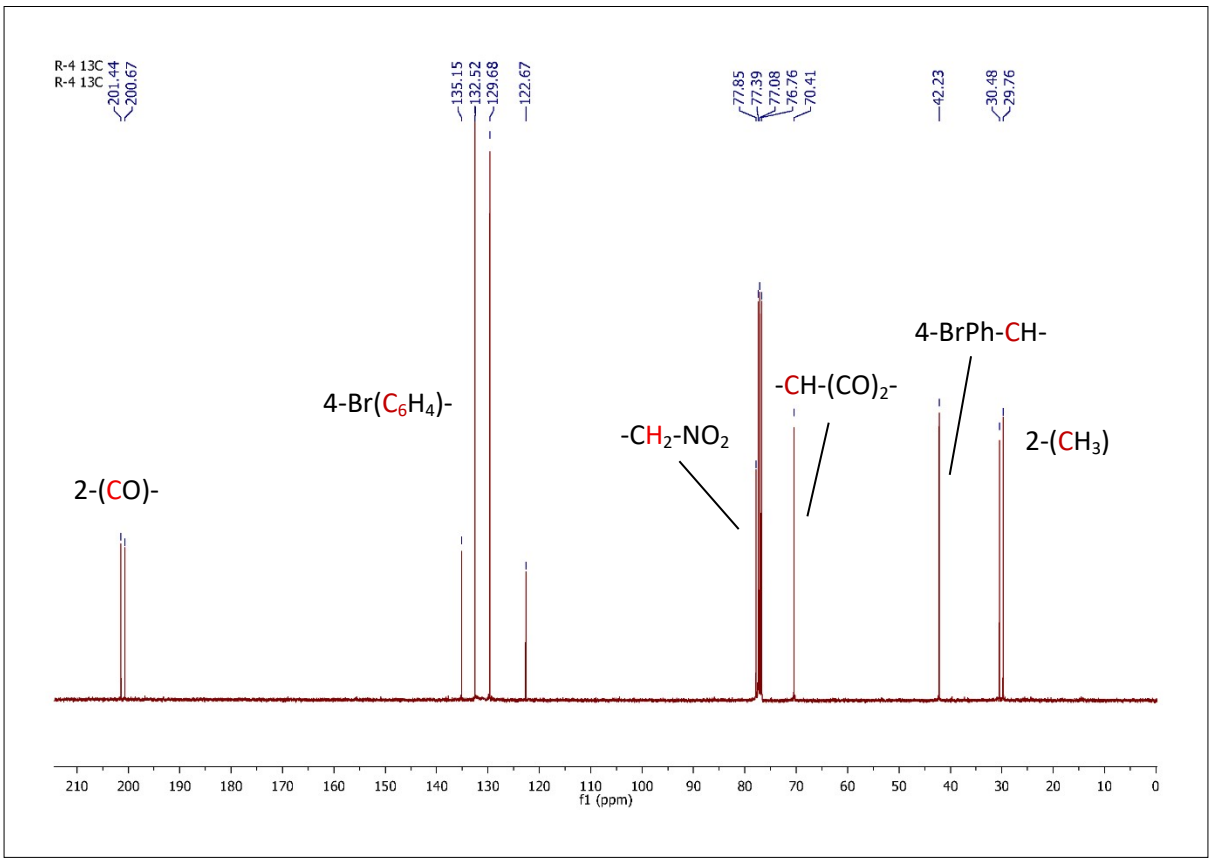

Figure S9: ^{1}H and ^{13}C NMR of **3bb** (Ethyl 2-acetyl-3-(4-bromophenyl)-4-nitrobutanoate).

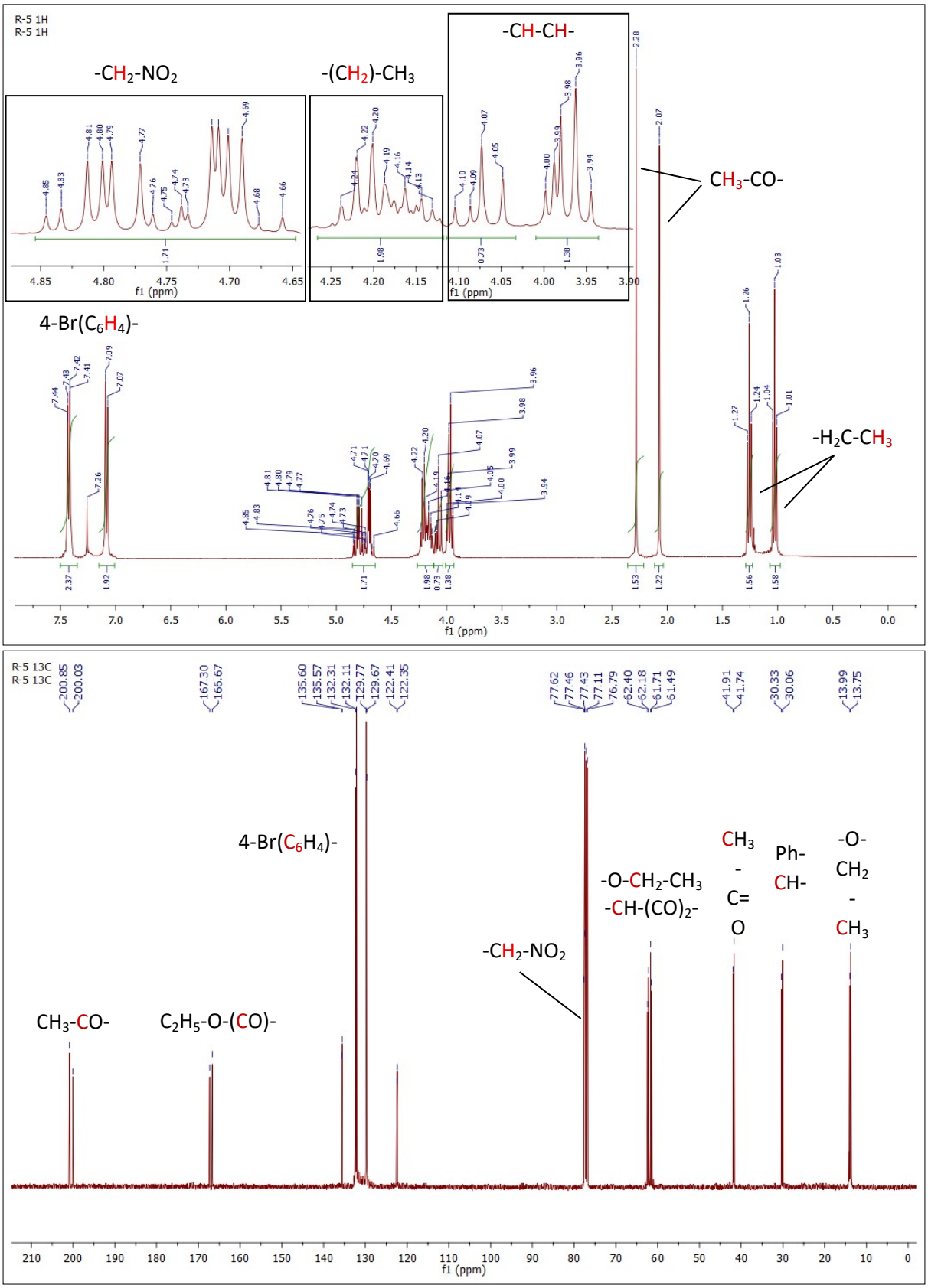

Figure S10: ^{1}H and ^{13}C NMR of 3cb (2-(1-(4-bromophenyl)-2-nitroethyl)malononitrile).

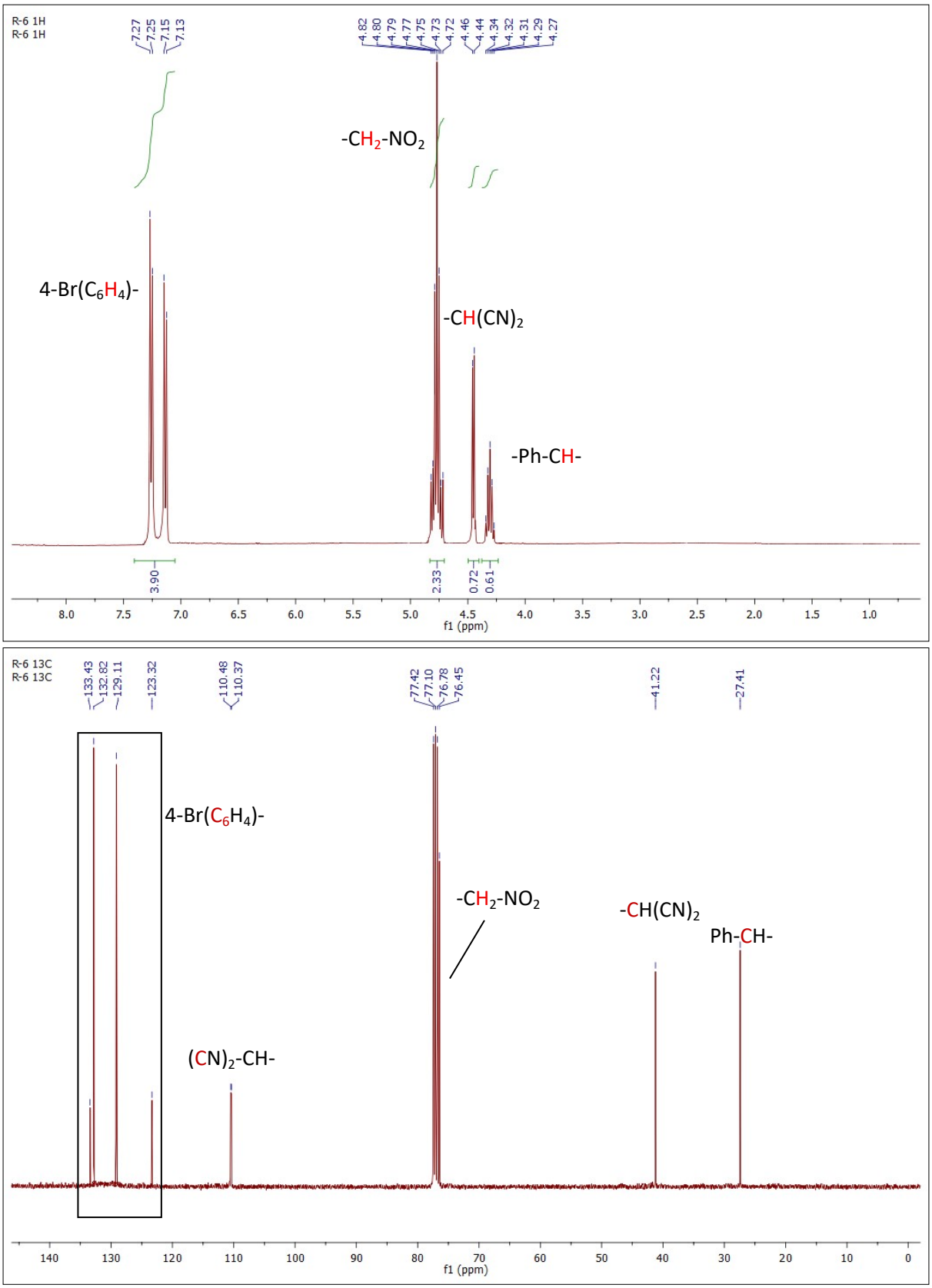

Figure S11: ^{1}H and ^{13}C NMR of **3ac** (3-(1-(2-chlorophenyl)-2-nitroethyl)pentane-2,4-dione).

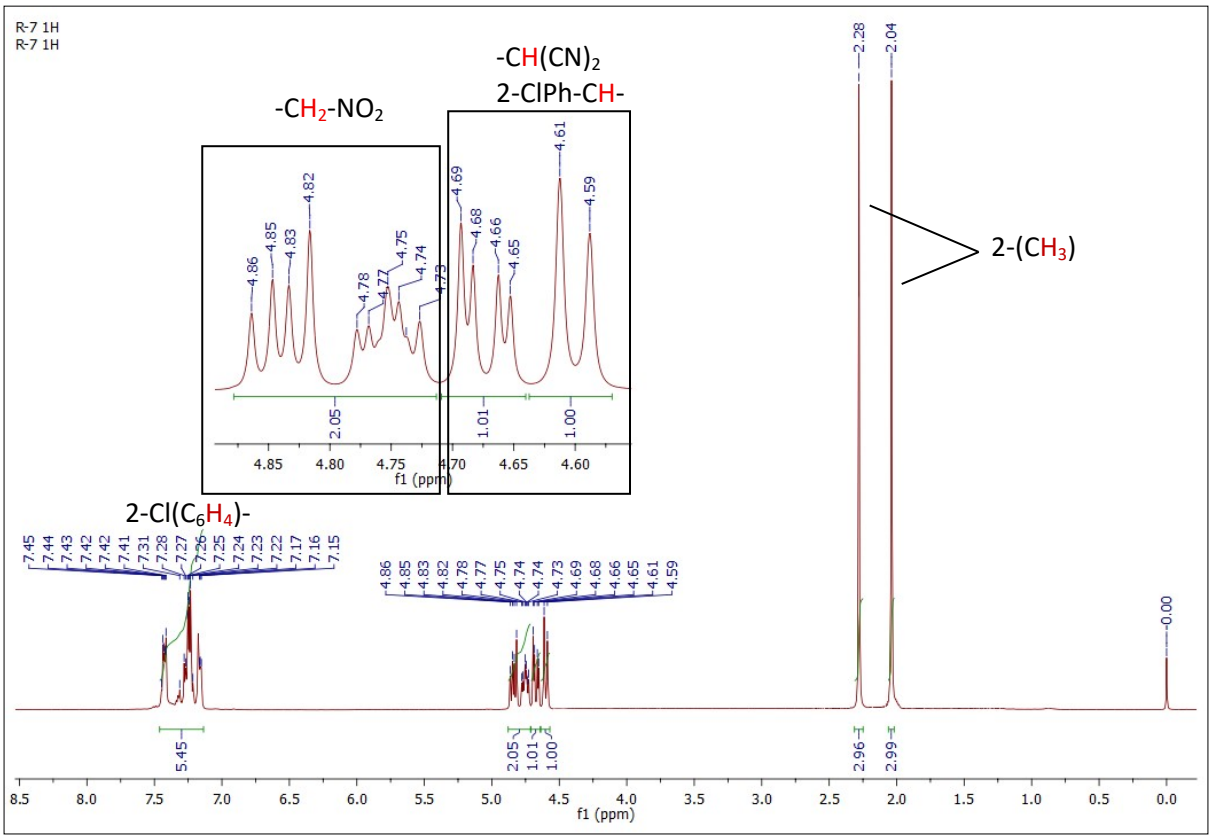

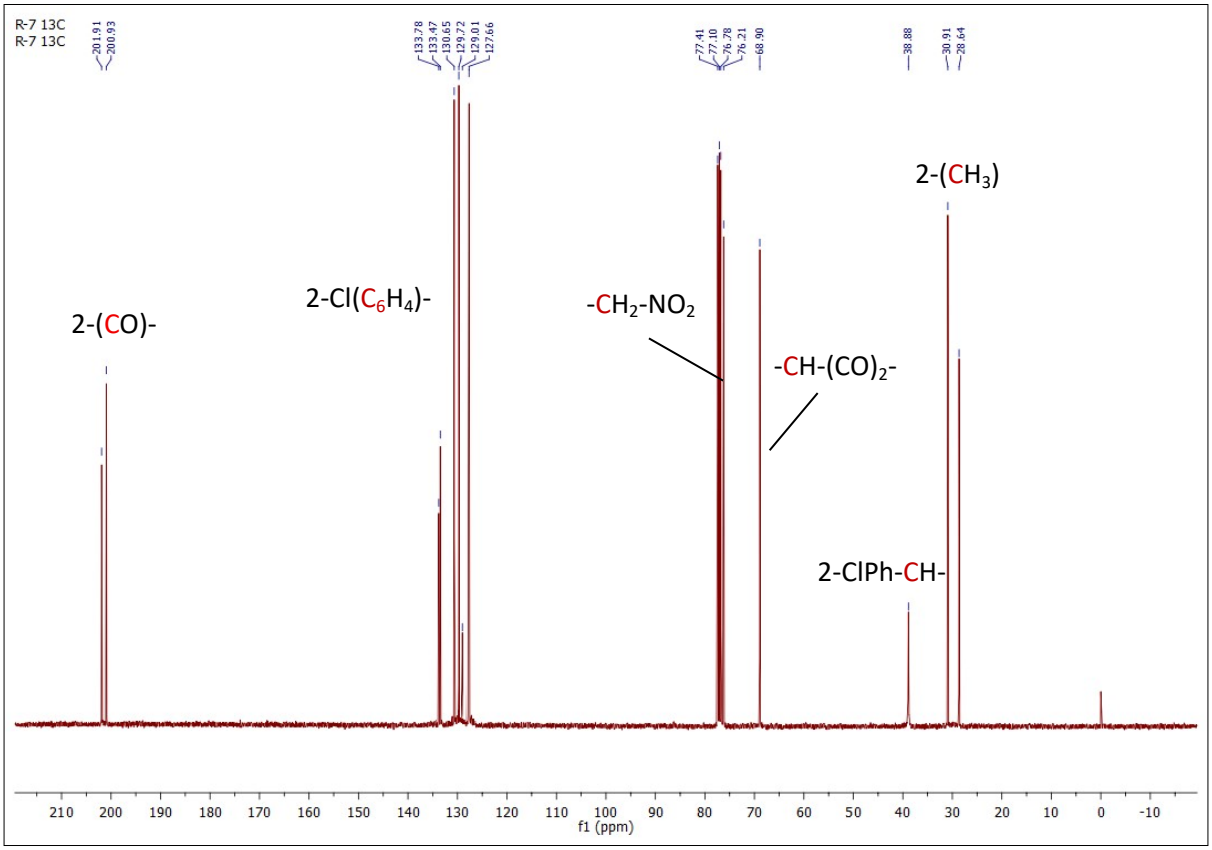

Figure S12: ^{1}H and ^{13}C NMR of **3bc** (Ethyl 2-acetyl-3-(2-chlorophenyl)-4-nitrobutanoate).

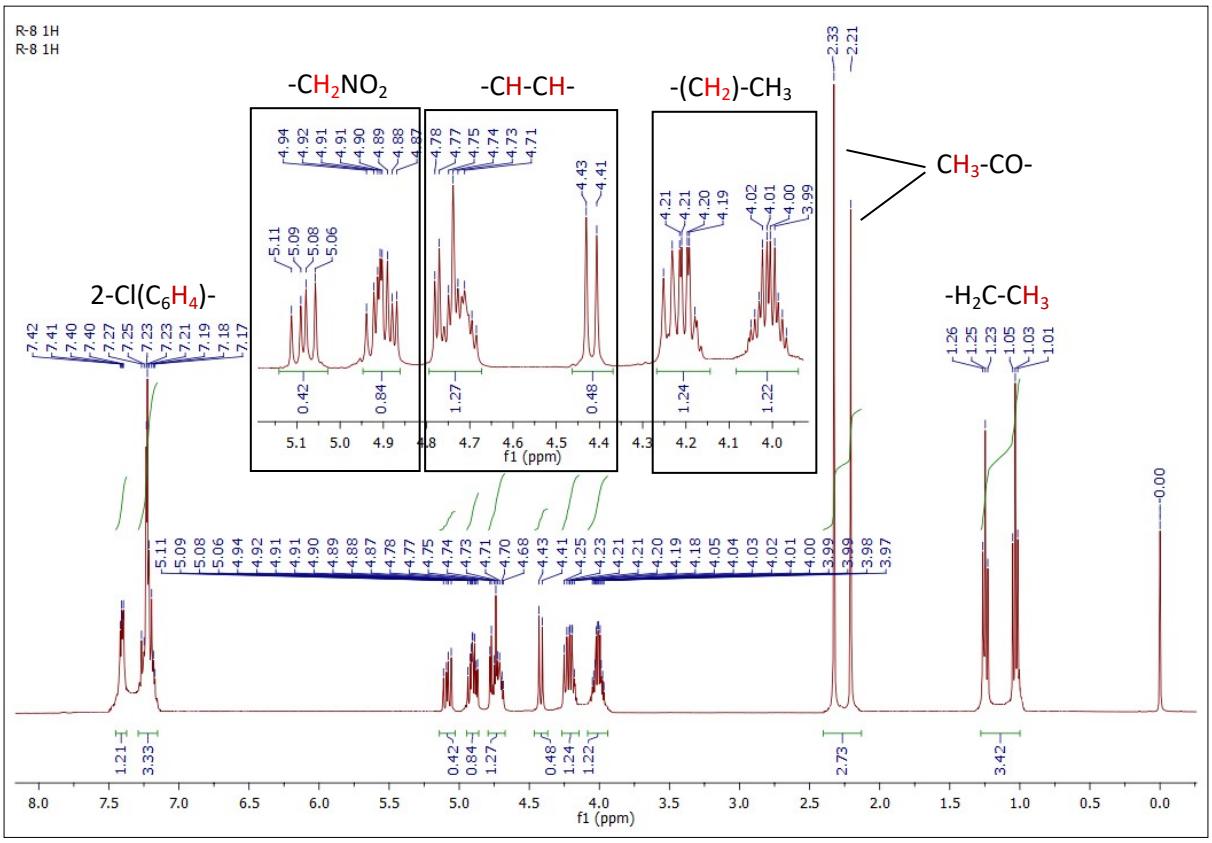

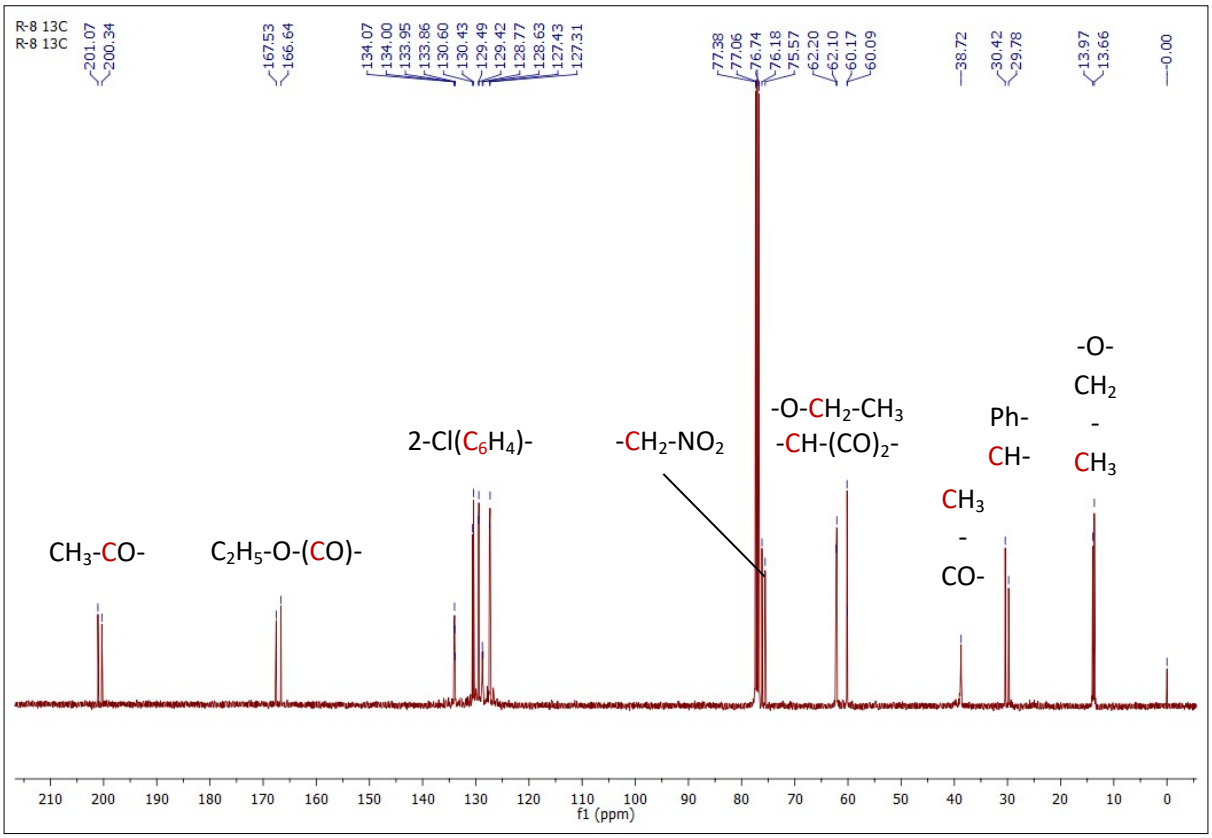

Figure S13: ^{1}H and ^{13}C NMR of **3cc** (2-(1-(2-chlorophenyl)-2-nitroethyl)malononitrile).

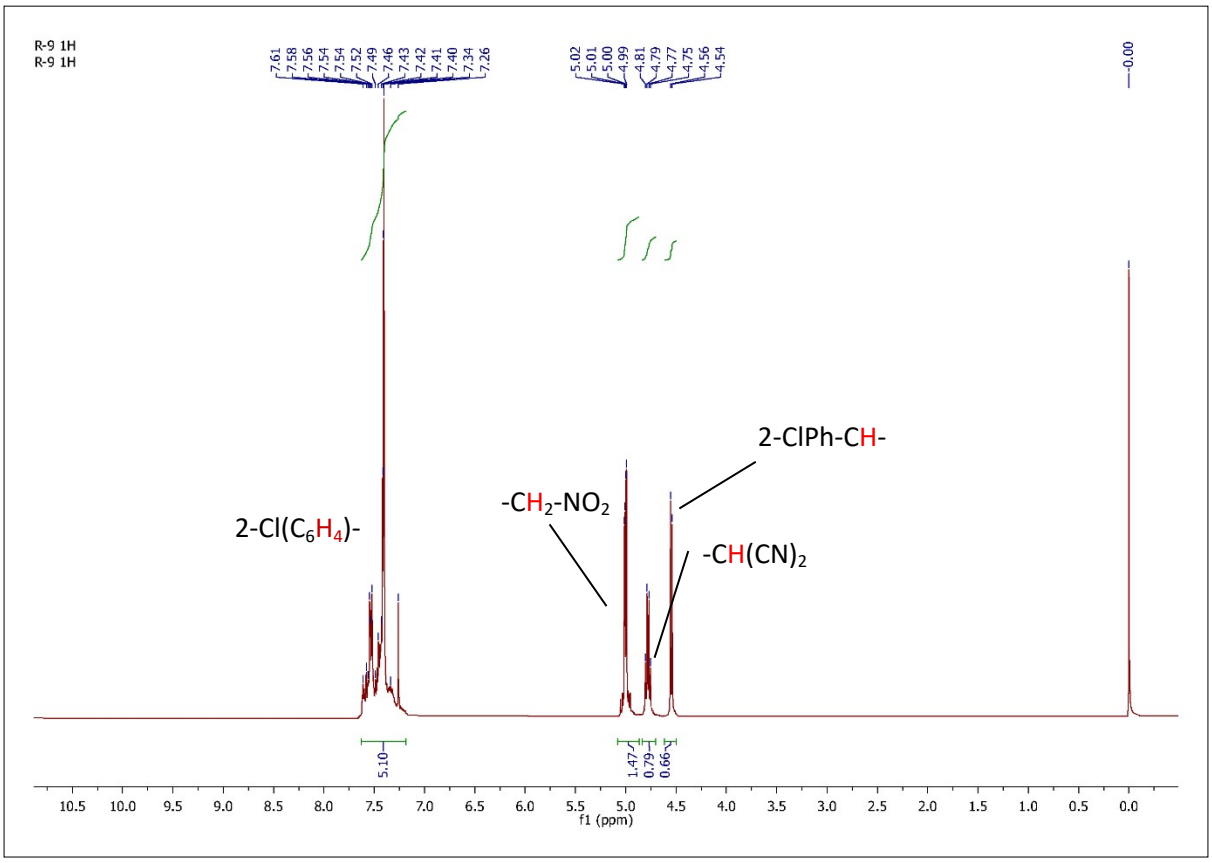

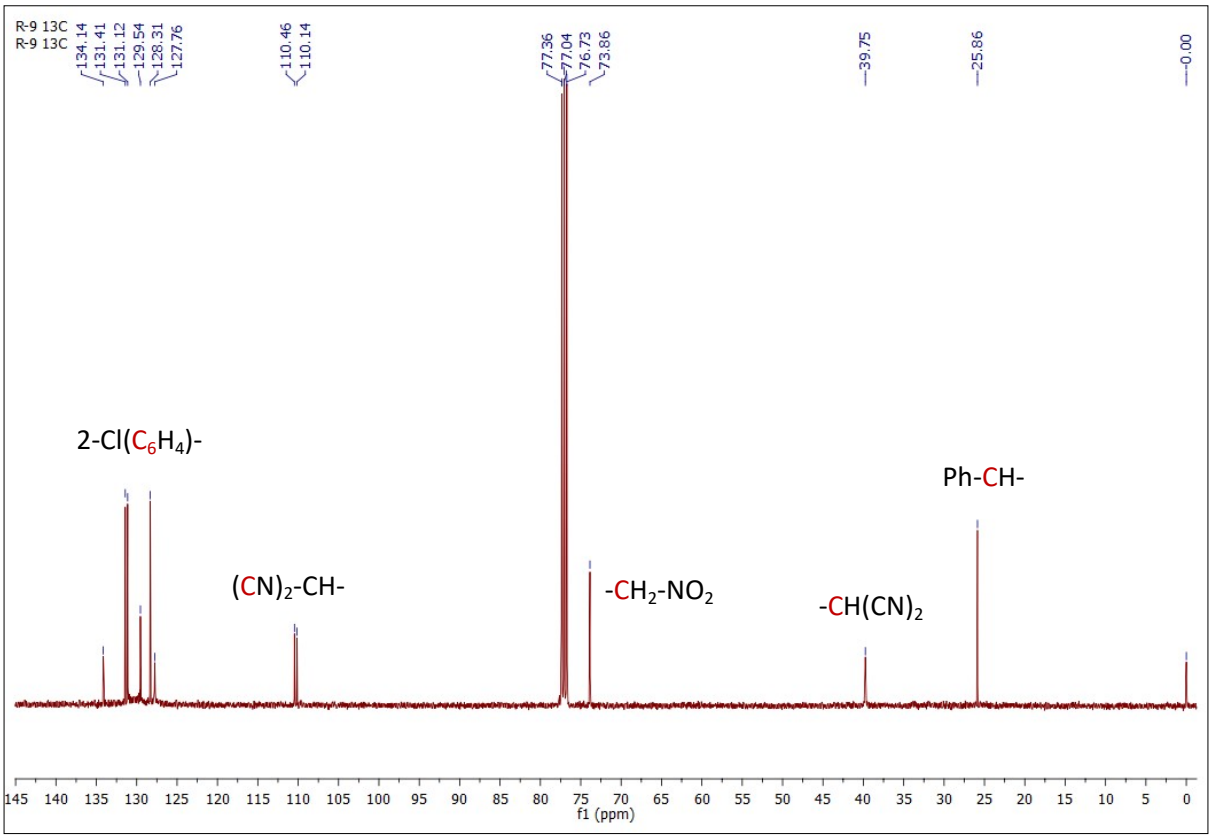

Figure S14: ^{1}H and ^{13}C NMR of **3ad** (3-(1-(4-chlorophenyl)-2-nitroethyl)pentane-2,4-dione).

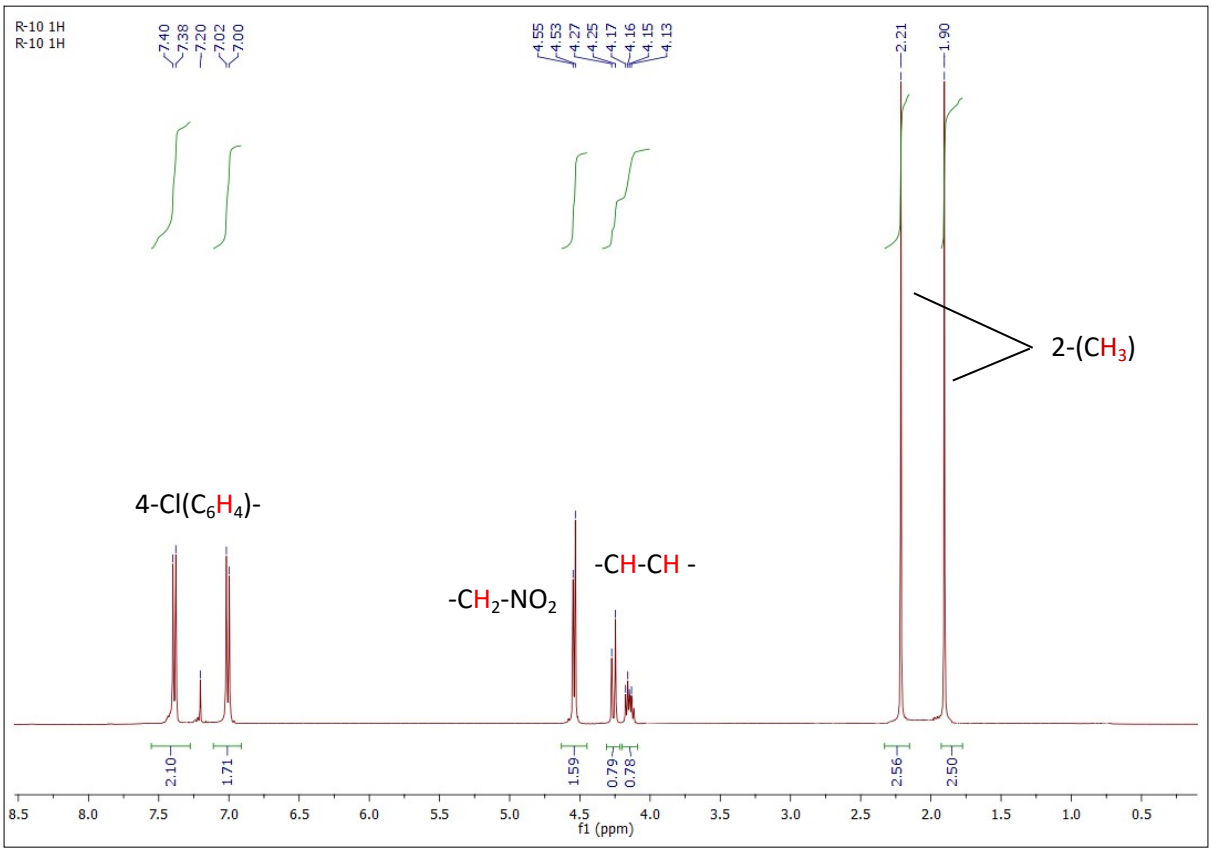

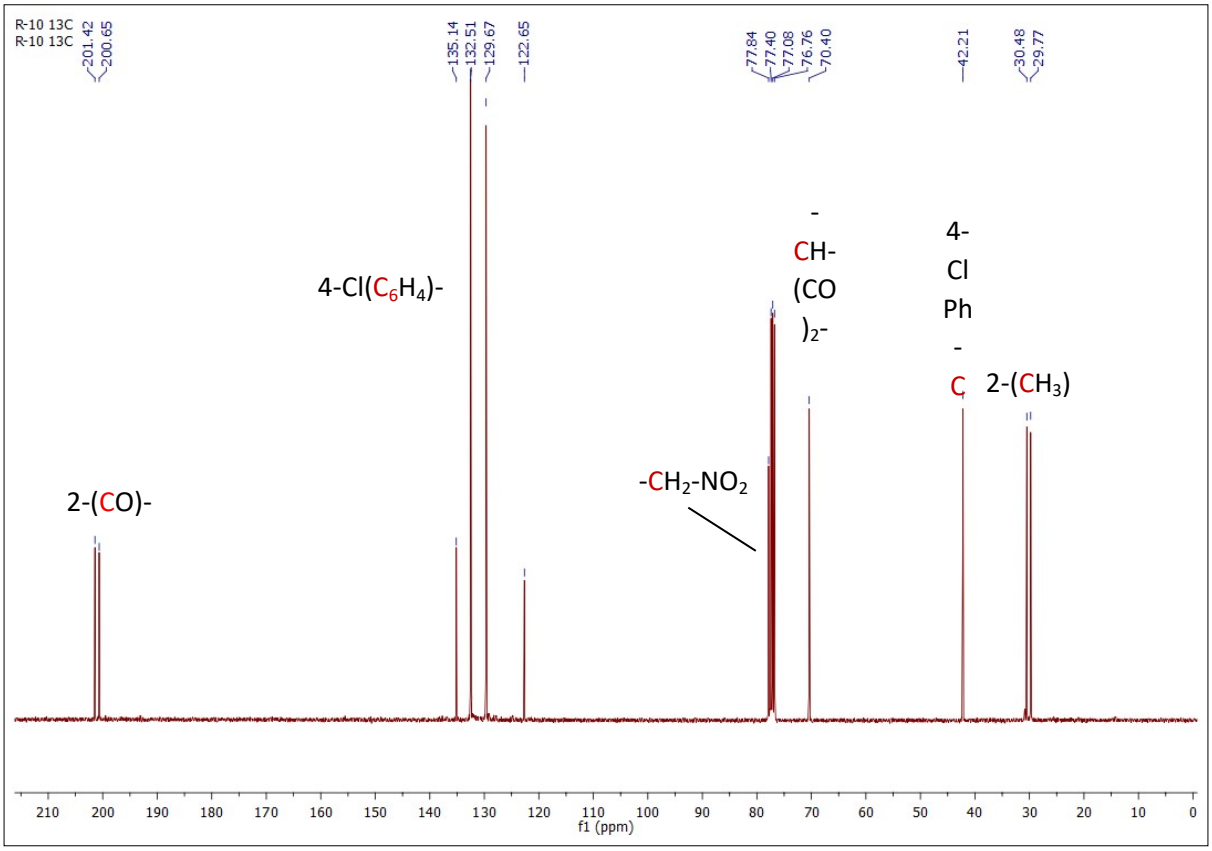

Figure S15: ^{1}H and ^{13}C NMR of **3bd** (Ethyl 2-acetyl-3-(4-chlorophenyl)-4-nitrobutanoate).

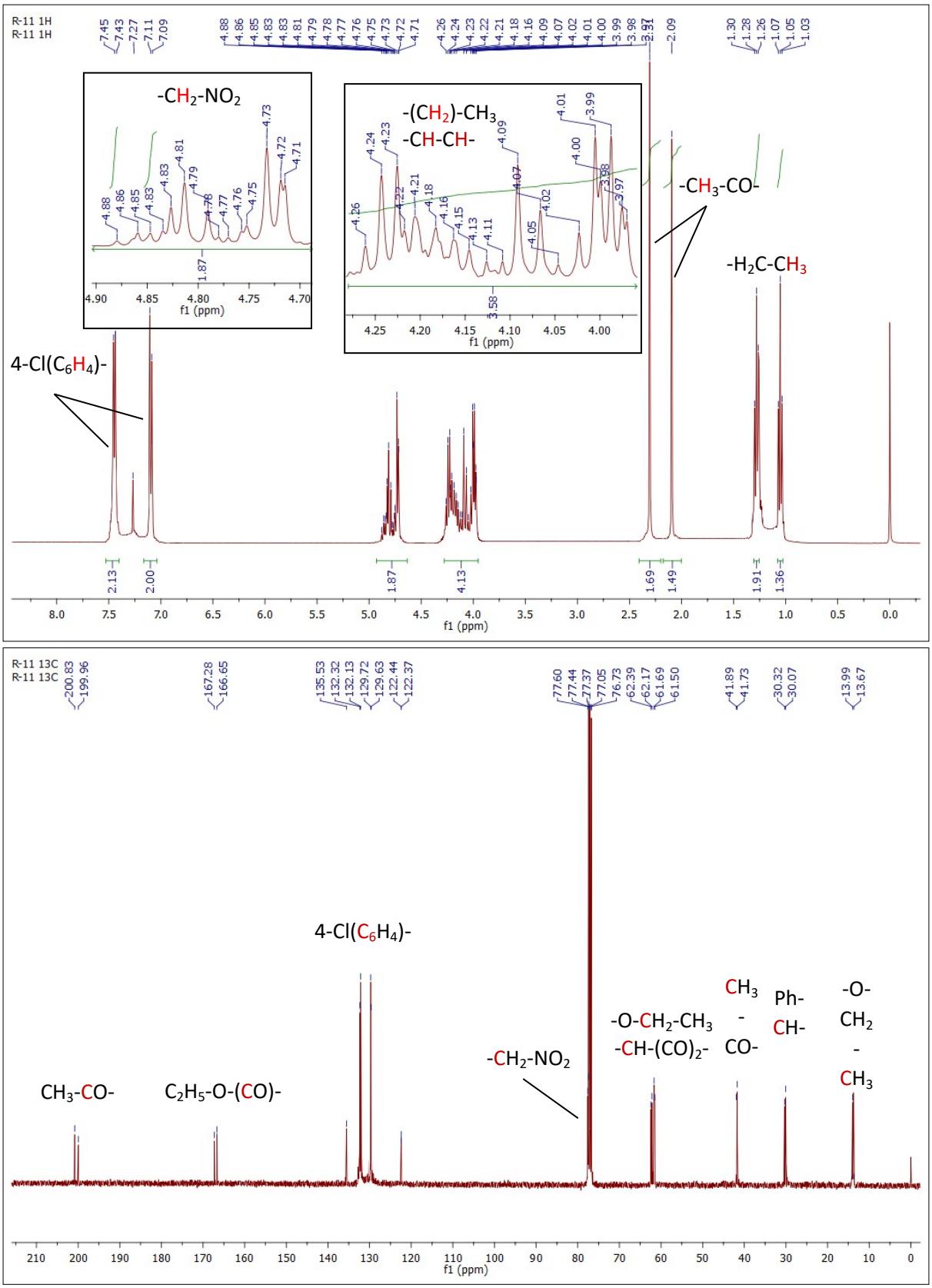

Figure S16: ^{1}H and ^{13}C NMR of **3cd** (2-(1-(4-chlorophenyl)-2-nitroethyl)malononitrile).

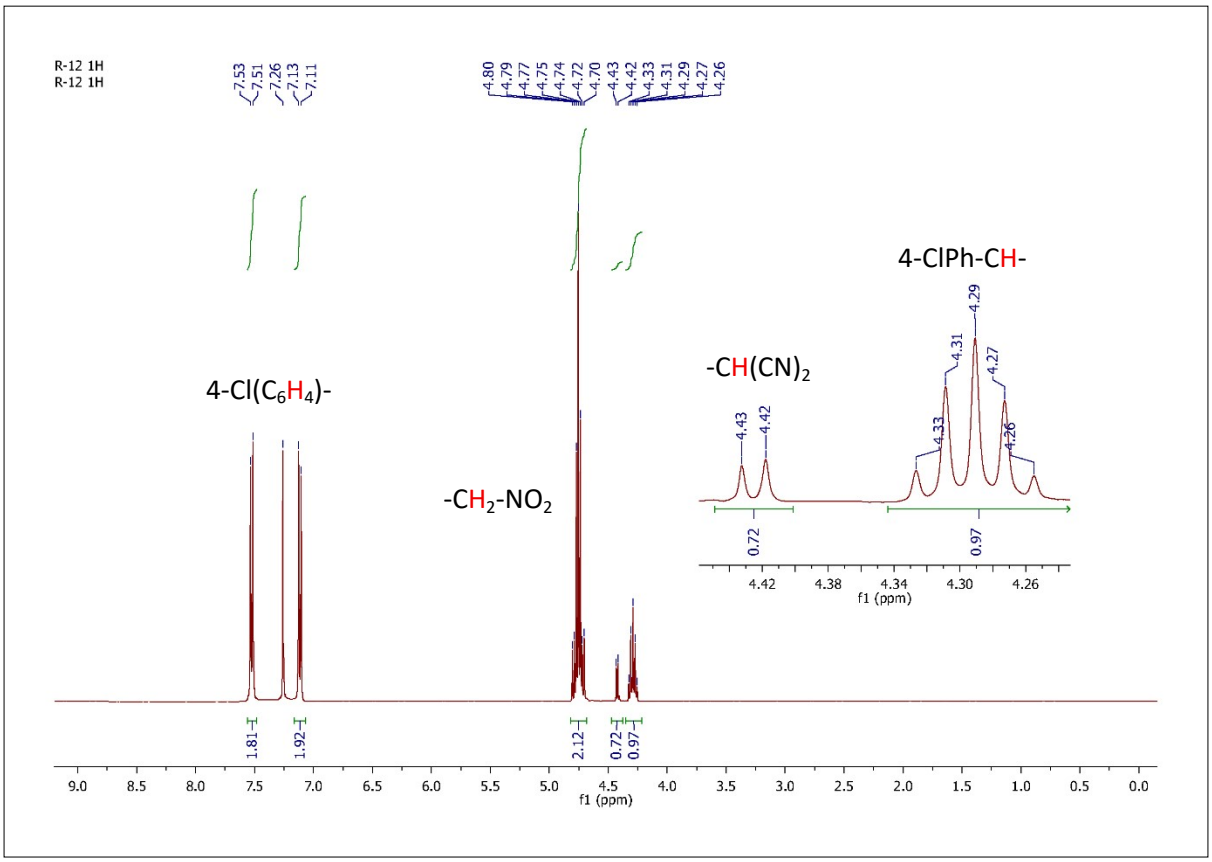

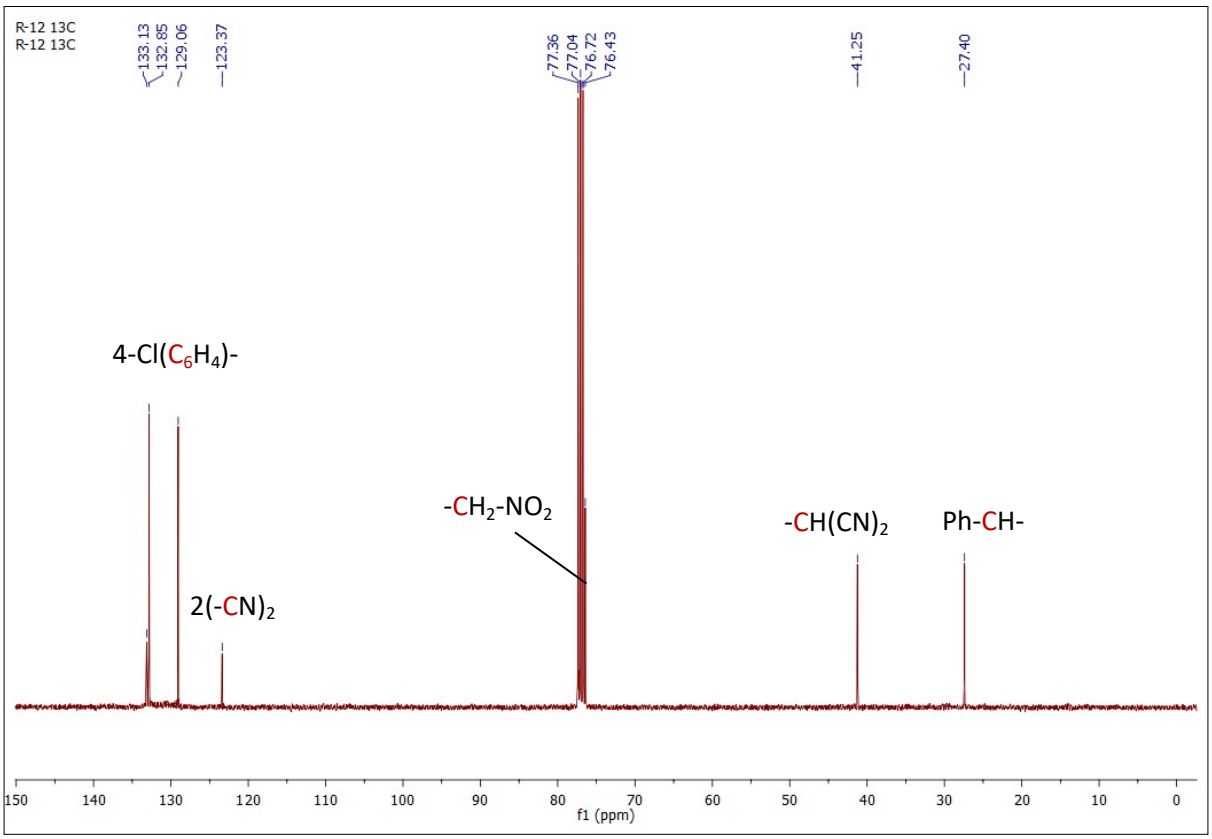

Figure S17: ^{1}H and ^{13}C NMR of **3ae** (3-(2-nitro-1-(p-tolyl)ethyl)pentane-2,4-dione).

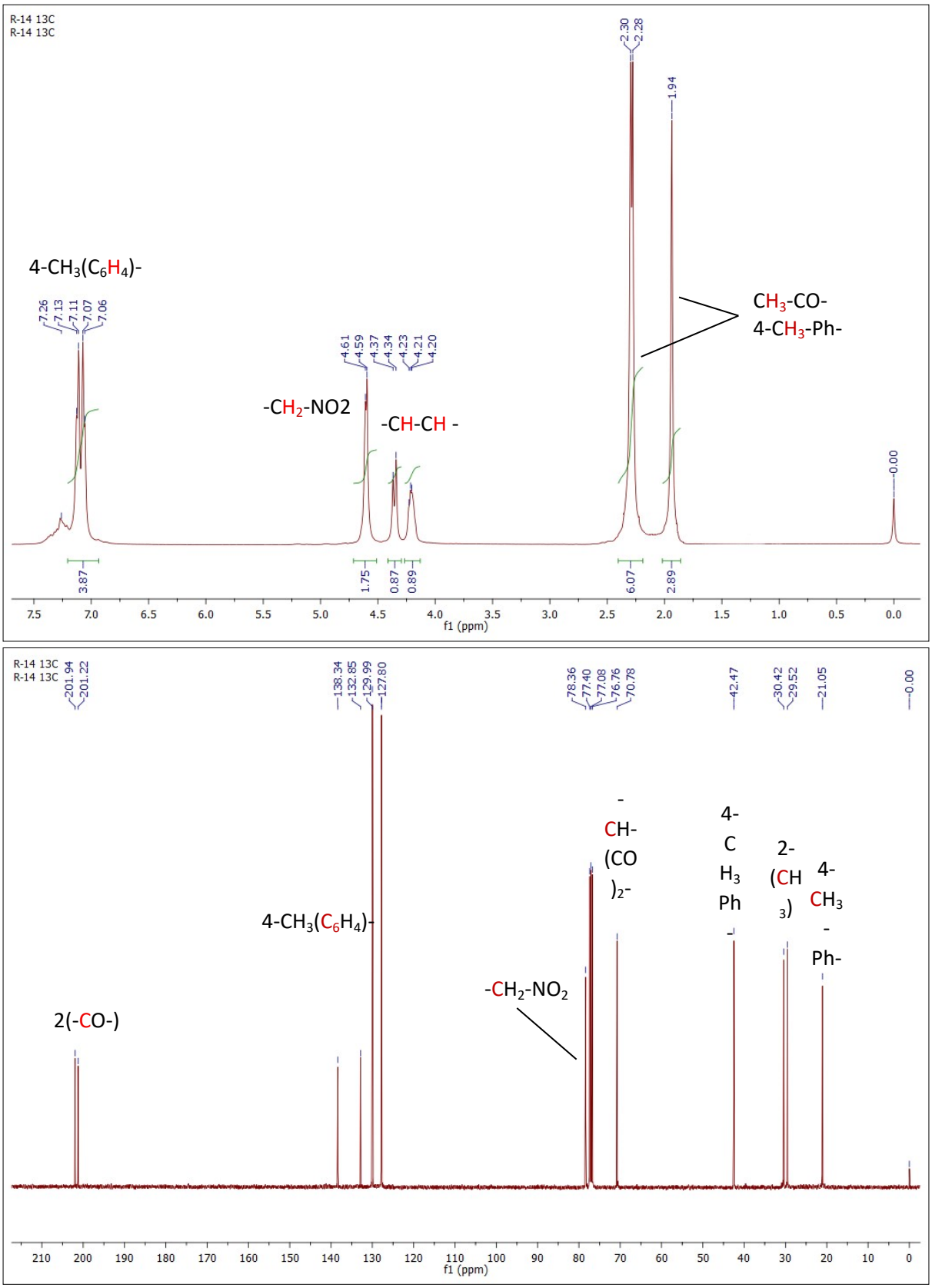

Figure S18: ^{1}H and ^{13}C NMR of **3be** (Ethyl 2-acetyl-4-nitro-3-(p-tolyl)butanoate).

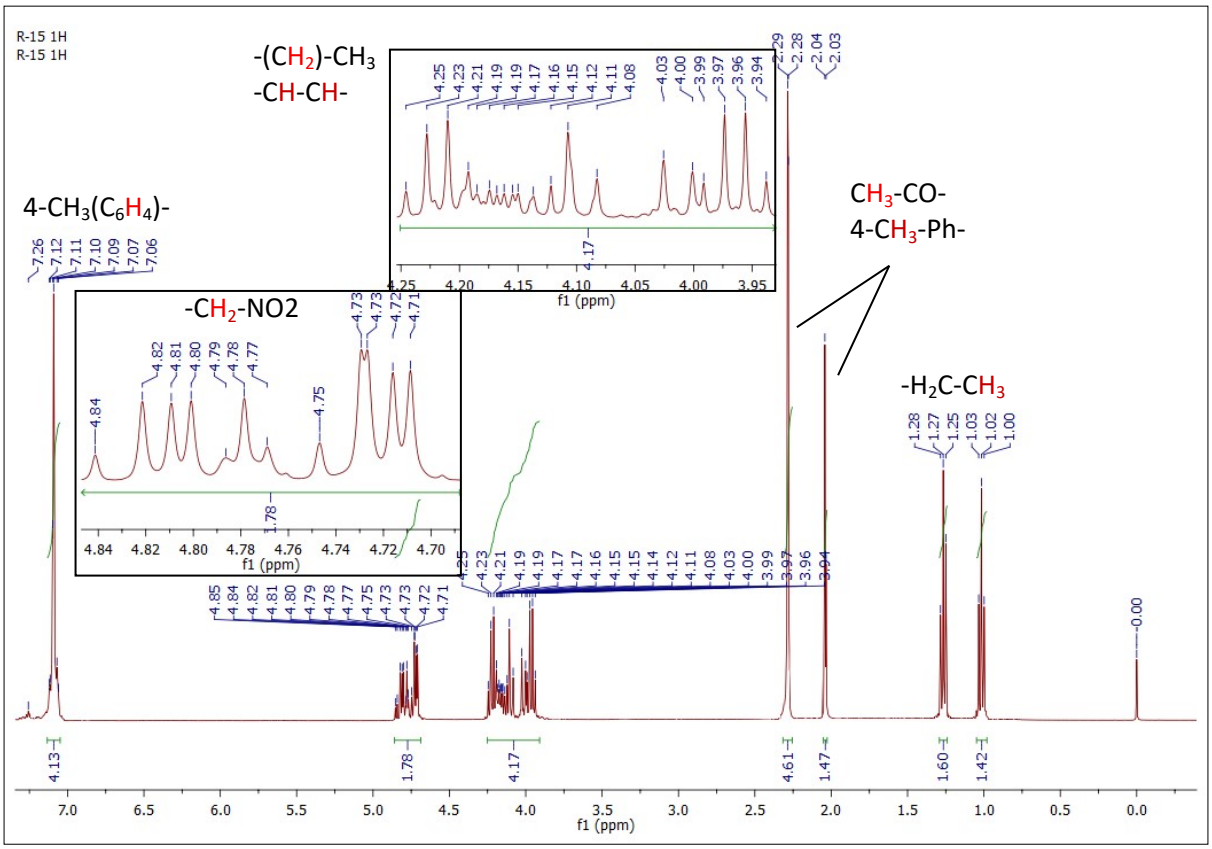

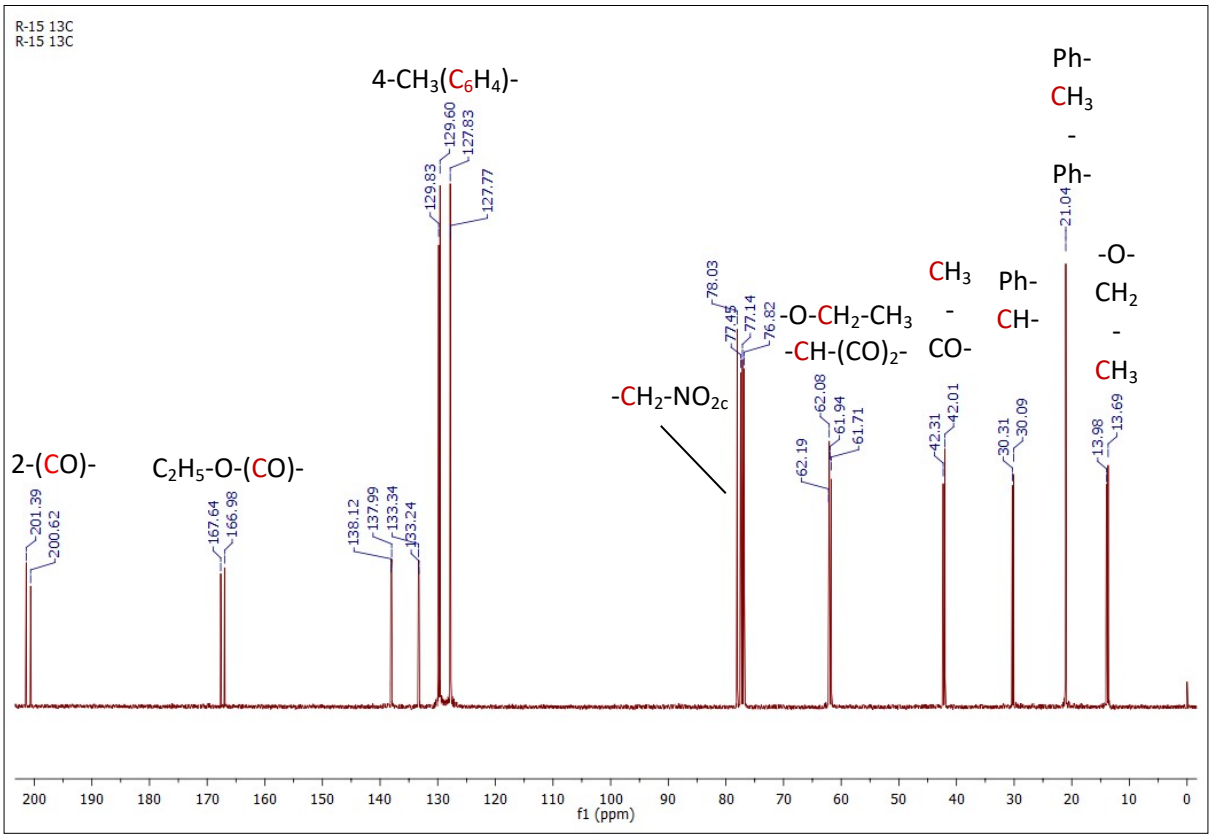

Figure S19: ^{1}H and ^{13}C NMR of **3ce** (2-(2-nitro-1-(p-tolyl)ethyl)malononitrile).

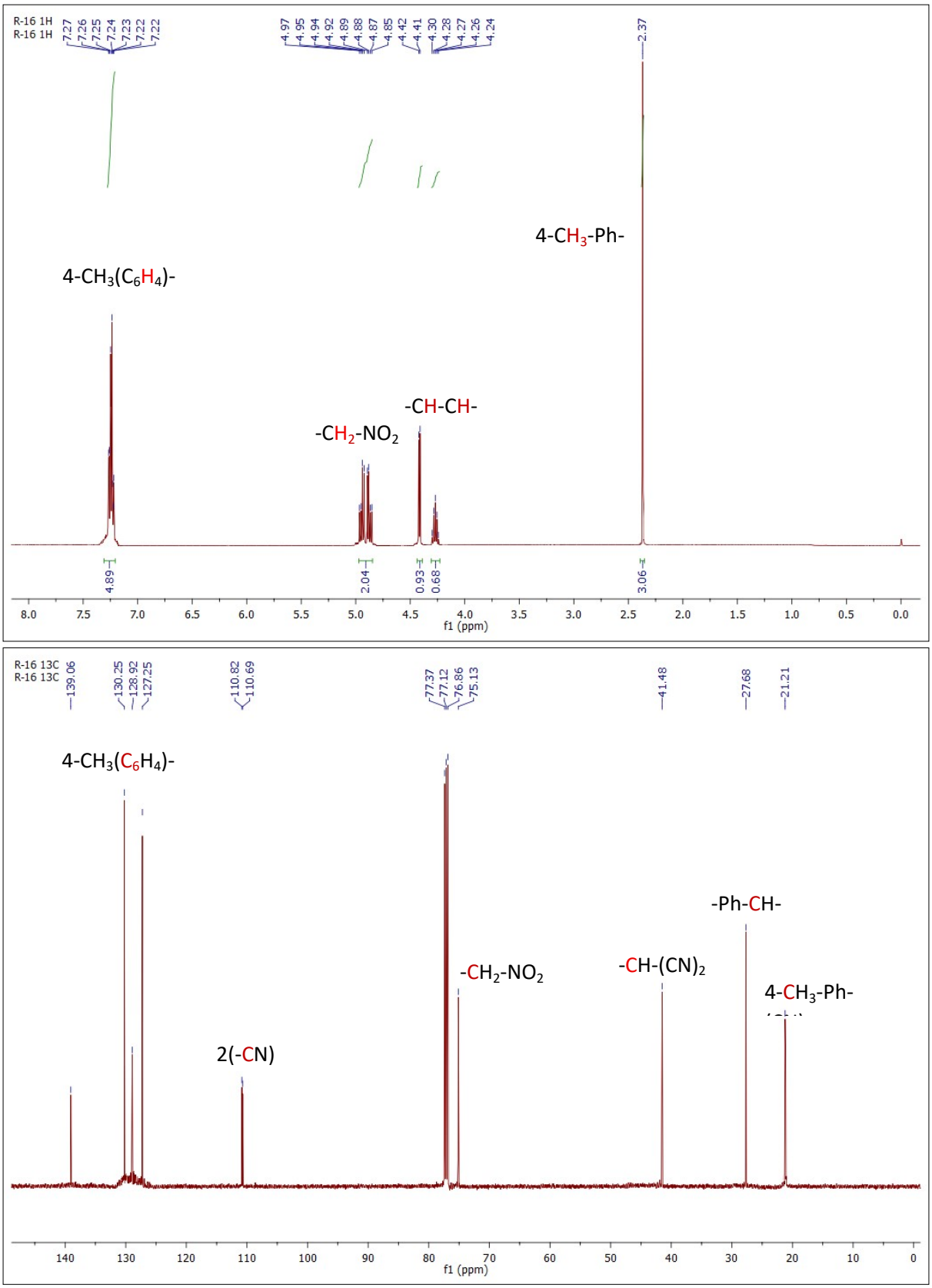

Figure S20: ^{1}H and ^{13}C NMR of **3af** (3-(1-(2-methoxyphenyl)-2-nitroethyl)pentane-2,4-dione).

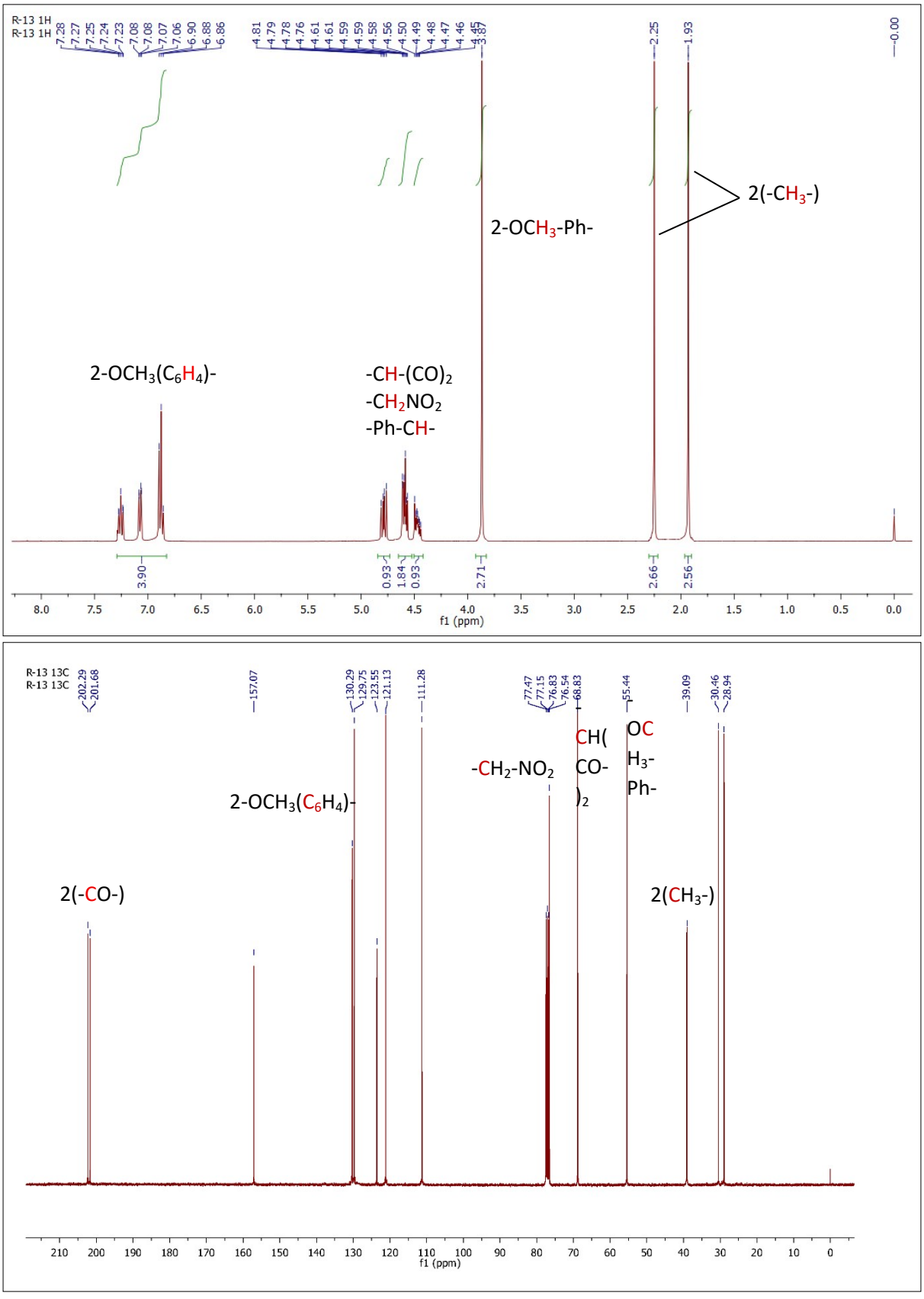

Table S2: Reusability of DFPA catalyst for Methanolysis of PET waste

Cycle	Time (h)	Catalyst Mas Loss	Yield (%)
1st	0.97	0.0326	98.64
2nd	1	0.0331	96.32
3rd	1.25	0.0329	94.72
4th	1.5	0.0325	93.15
5th	2	0.0341	91.46
6th	2.25	0.0337	90.48
7th	2.42	0.0334	88.49
8th	2.5	0.03425	87.13
9th	2.7	0.0329	86.21
10th	2.9	0.0332	84.56

Figure S21: EDX analysis of DFPA after 5th cycle

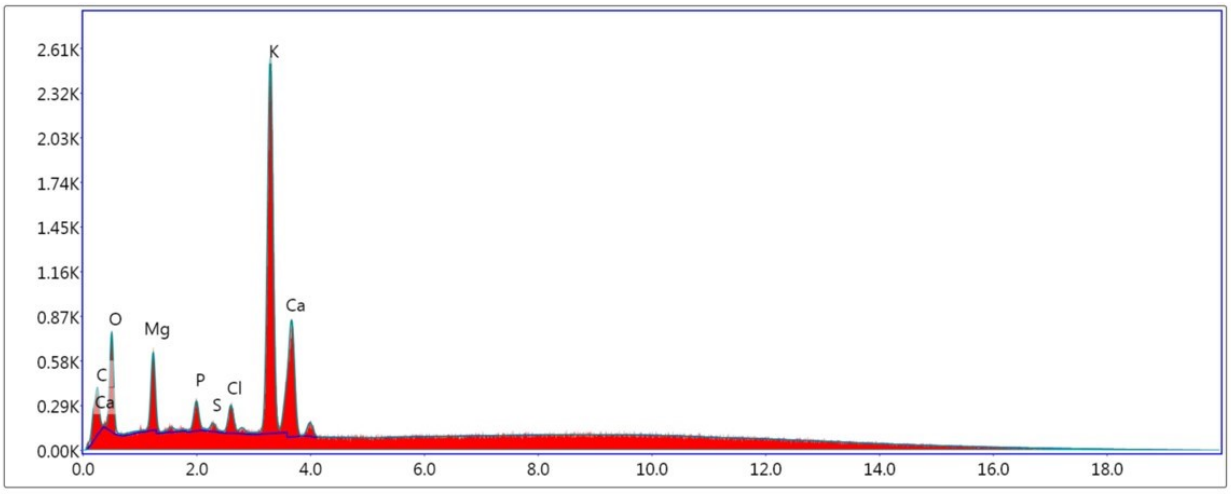

Lsec: 30.0 0 Cnts 0.000 keV Det: Octane Plus Det

Element	Weight %	Atomic %	Net Int.	Error %	Kratio	Z	R	A	F
C K	4.98	9.41	45.77	13.83	0.02	1.12	0.93	0.32	1
O K	39.55	56.12	321.24	11.01	0.05	1.08	0.96	0.13	1
MgK	5.68	5.31	295.63	8.51	0.03	1	0.99	0.48	1.01
P K	1.85	1.35	130.49	8.75	0.01	0.94	1.01	0.81	1.03
S K	0.45	0.32	34.46	26.31	0.00	0.96	1.02	0.87	1.05
ClK	1.78	1.14	131.36	13.02	0.02	0.92	1.02	0.92	1.08
K K	32.08	18.63	1,936.14	1.99	0.29	0.91	1.04	0.97	1.03
CaK	13.64	7.73	594.11	4.51	0.11	0.93	1.04	0.85	1

Figure S22: EDX analysis of DFPA catalyst after 10th cycle

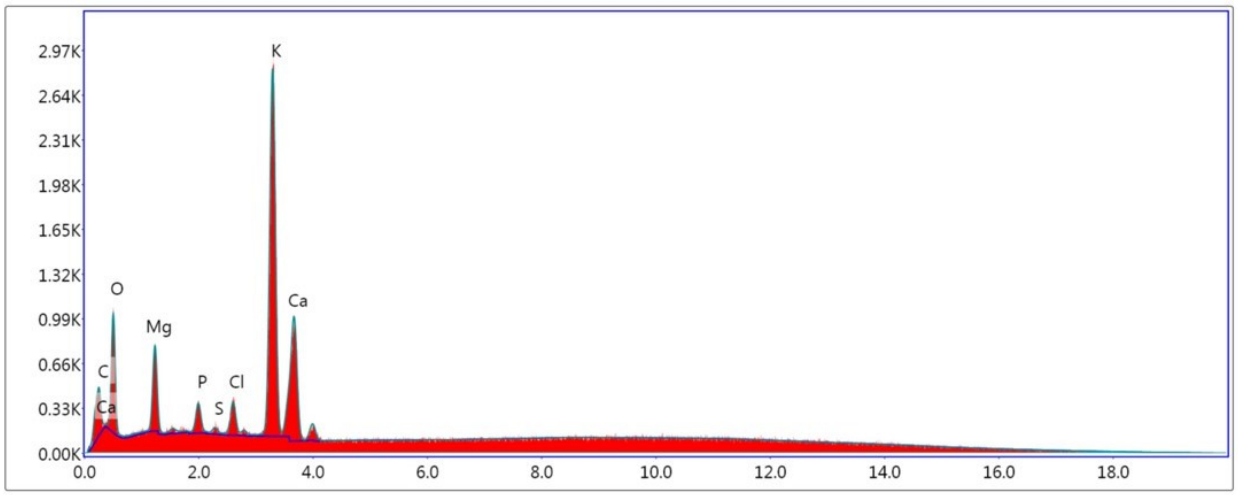

Lsec: 30.0 0 Cnts 0.000 keV Det: Octane Plus Det

Element	Weight %	Atomic %	Net Int.	Error %	Kratio	Z	R	A	F
C K	5.30	9.76	58.55	13.45	0.02	1.12	0.94	0.32	1
O K	42.27	58.38	440.96	10.76	0.06	1.07	0.96	0.13	1
MgK	5.86	5.32	369.46	8.19	0.03	0.99	0.99	0.47	1.01
P K	1.73	1.23	147.51	8.40	0.01	0.94	1.01	0.81	1.03
S K	0.32	0.22	30.31	35.70	0.00	0.96	1.02	0.87	1.05
ClK	1.99	1.24	177.87	10.92	0.02	0.91	1.03	0.92	1.08
K K	29.28	16.54	2,148.10	1.97	0.27	0.91	1.04	0.97	1.03
CaK	13.25	7.31	710.43	4.14	0.11	0.92	1.04	0.86	1

Figure S23: SEM images of 5th (a) and 10th (b) cycle

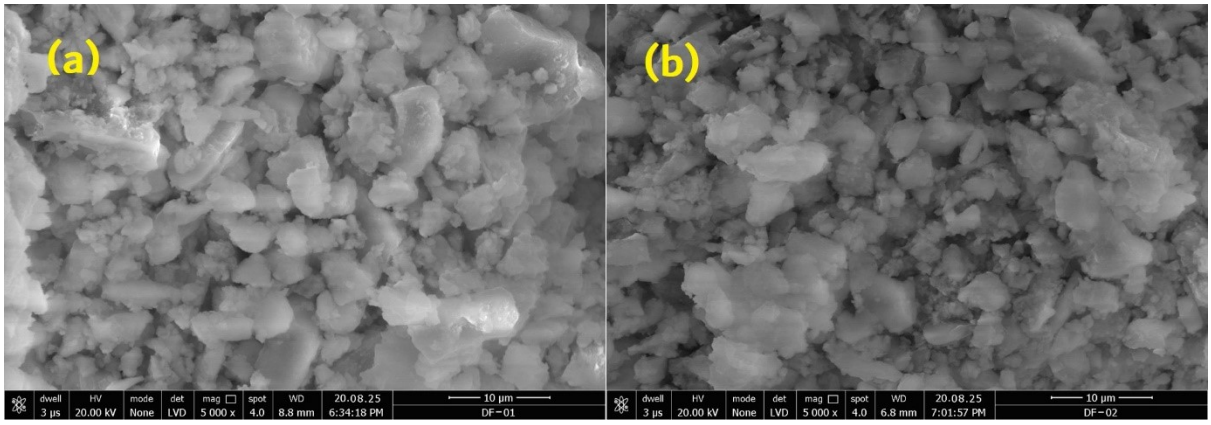

Figure S24: HPLC data of crude methanolysis product

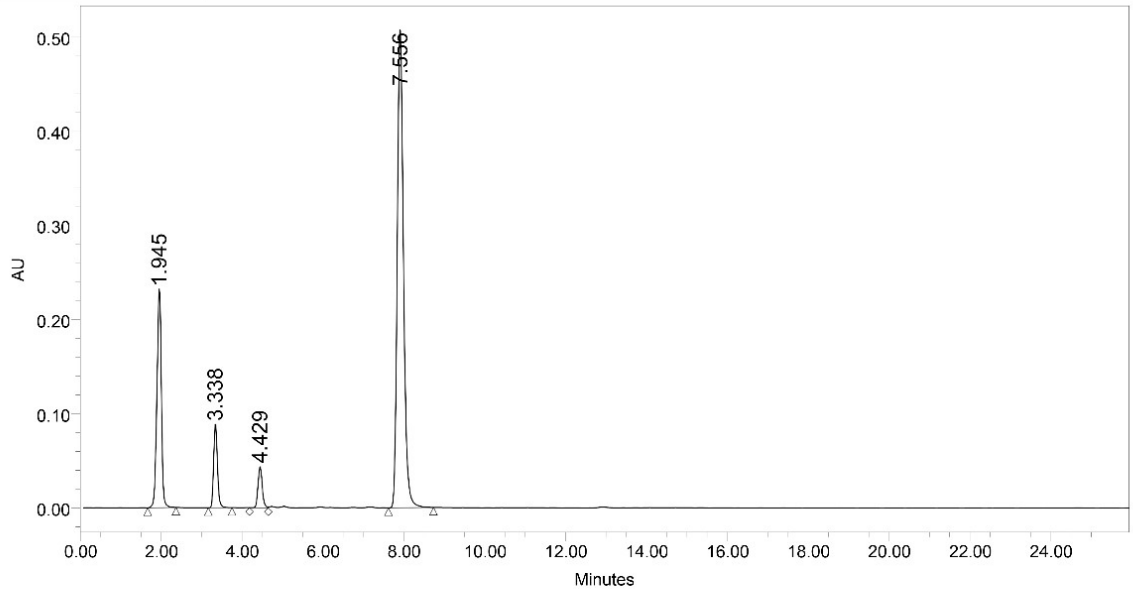

	RT (min)	Area (µV*sec)	% Area	Height (µV)	% Height
1	1.945	1878457	22.4	237014	26.57
2	3.338	585112	6.93	89348	10.02
3	4.429	321168	3.88	43772	4.91
4	7.556	5598973	66.79	521936	58.51

Figure S25: HPLC data of recrystallized methanolysis product

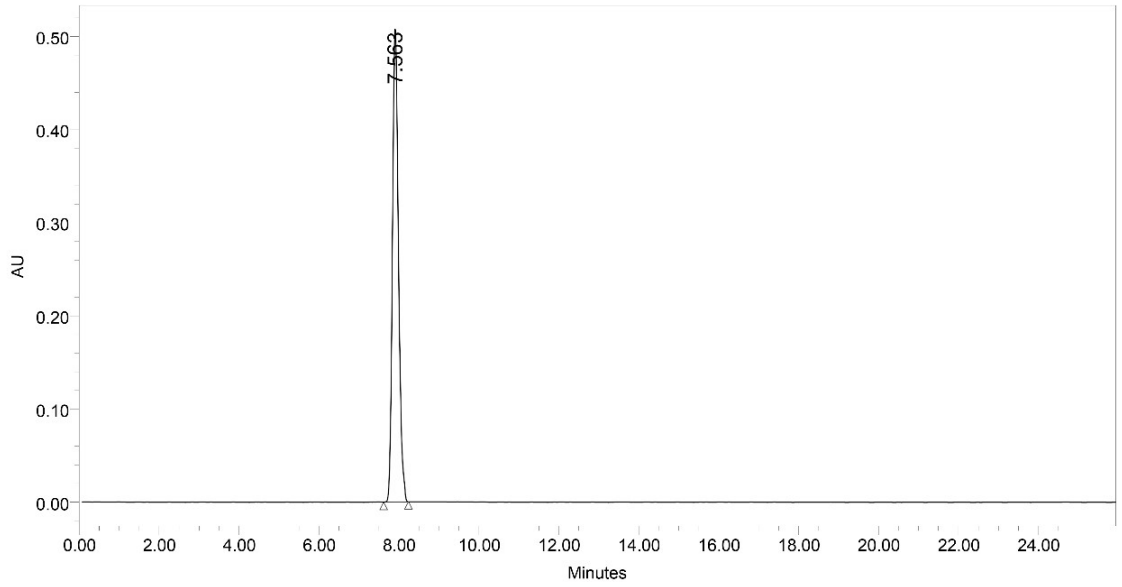

	RT (min)	Area (µV*sec)	% Area	Height (µV)	% Height
1	7.563	9560912	100.00	510720	100.00

Figure S26: FT-IR Spectra of methanolysis product

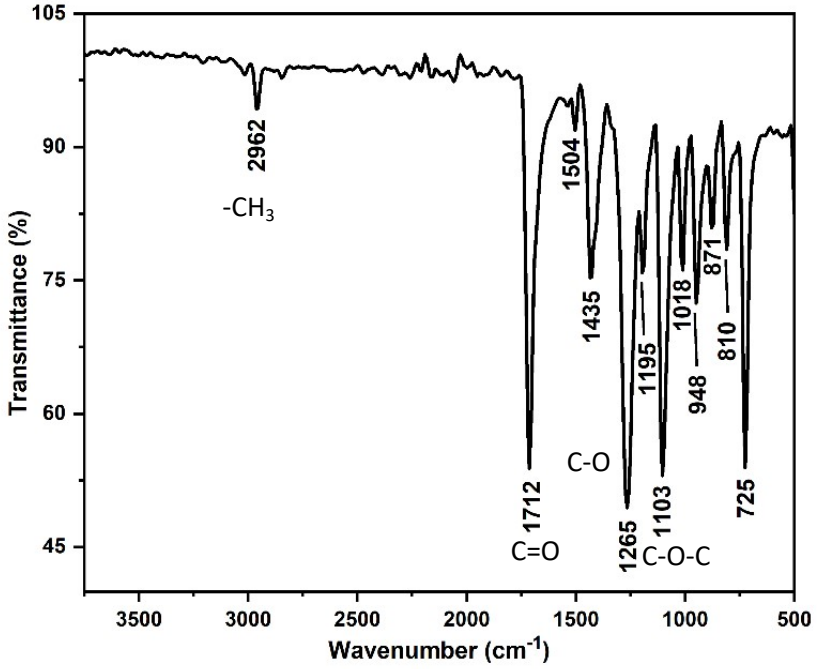

Figure S27: ^{13}C NMR spectra of DMT

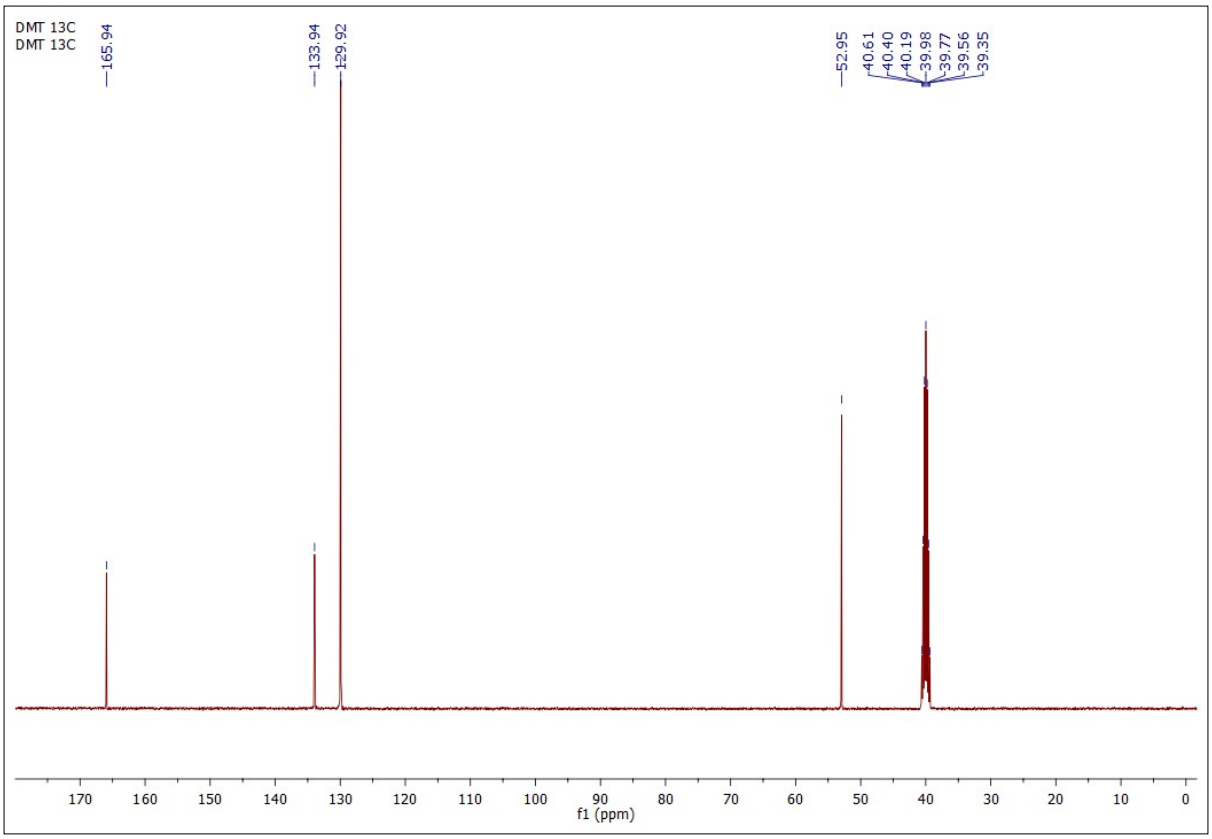

Figure S28: (a) Leverage vs run plot. (b) Residuals vs run plot

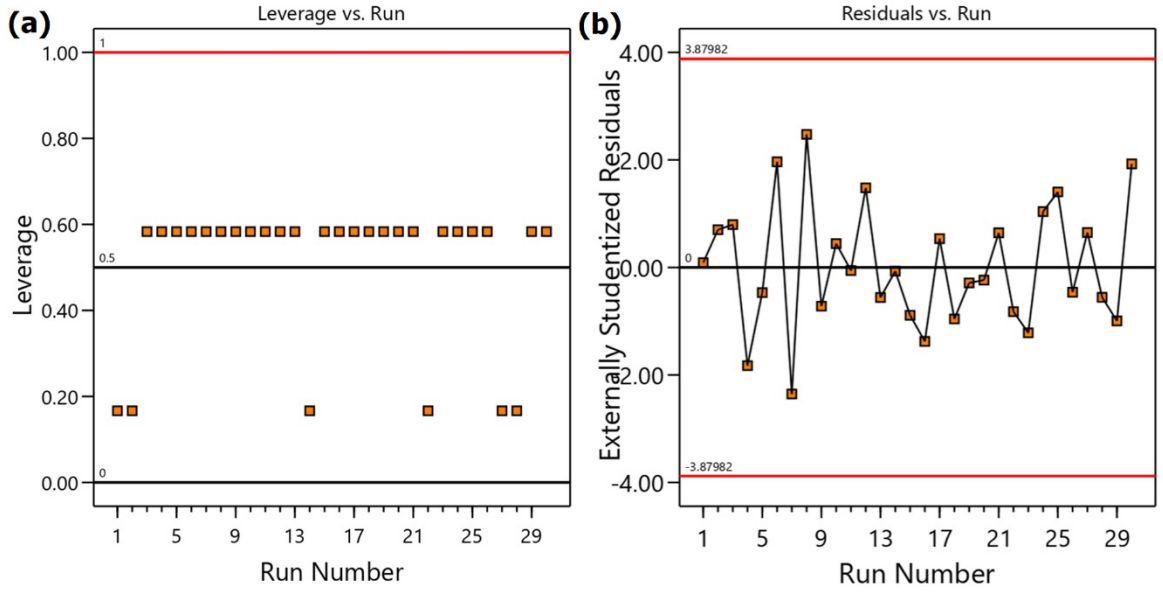

Table S3: Methanolysis data of colored and labeled PET

S/No.	PET	Recrystallized Yield (%)
1.	Blue	96.15±0.43%

2.	Green	95.84±0.51%
3.	Red	95.73±0.62%
4.	Label	91.52±0.58%

Figure S29: (a) UV spectra of colored PET solution. (b) UV spectra of recrystallized colored DMT

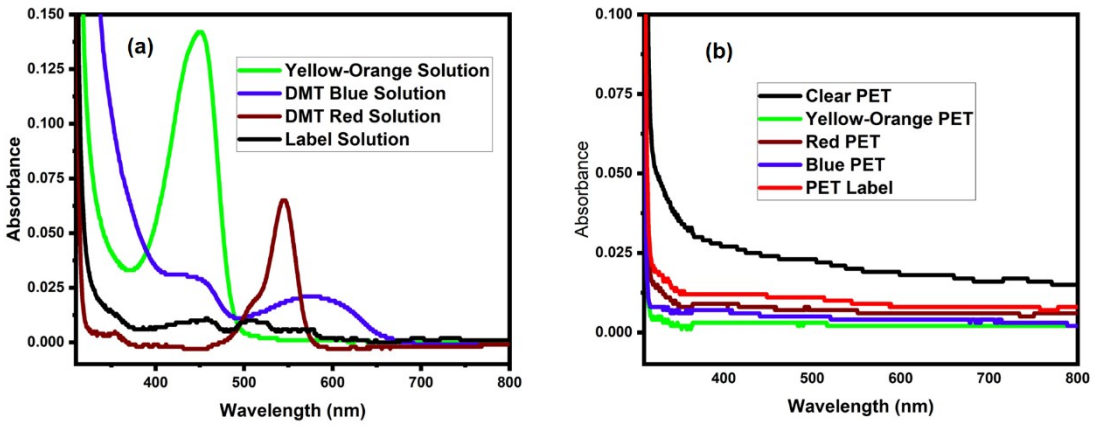

Table S4: Determination of Energy Input in kWh/Kg(DMT) on methanolysis

A.	**Determination of Total kWh for PET Depolymerization up to 0.01 Kg**				
1.	Equipments	Power (kW)	Time (h)	kWh	Total kWh
2.	Heating Mantle	0.698	1.25	0.8725	2.63
3.	Referigerator	0.09	4	0.36	
4.	Hot Air Oven	0.8	0.5	0.4	
5.	Rotary Evaporator	2	0.16	0.32	
B.	**Determination of kWh/DMT at low PET loading and Average Yield Percent**				
	PET loading	DMT (kg)	kWh/DMT (kg)	Yield%	Average Yield%
1.	0.0005	0.000498	5286.14	98.64	98.63
2.	0.001	0.000995	2645.73	98.46	
3.	0.005	0.00499	526.5	98.76	
4.	0.01	0.00997	264.04	98.66	

C.	Estimation of Total kWh for 1 Kg PET				
	Equipments	Power (kW)	Time (h)	kWh	Total kWh
1.	Heating Mantle	2.63	2	5.26	46.02
2.	Rotary Evaporator	2	20	40	
3.	Referigerator	0.09	4	0.36	
4.	Hot Air Oven	0.8	0.5	0.4	
D.	**Estimation of kWh/Kg (DMT) at 1 Kg PET loading.[a]**				
	Unit		Values		
1.	DMT Yield (Kg)		0.9863		
2.	kWh/Kg		46.66		

[a] DMT yield at 1 Kg PET was estimated from the average yield percent observed in entry B2.

	DMT A	**Byproducts B**	**Ethyl-ene Glycol C**	**Metha-nol D**	**Catal-yst Recov-ered**	**Total Mass Isolated [G = A+B+ C+D+E+]**	**Theo-retical Total Mass**	**Total Loss I = [H-**

Table S5: Green Metrics of Methanolysis reaction

S/N	Data	Methanol A	Catalyst B	DMT Yield C	Ethylene Glycol D	Oligomers E	Side Products F	Total Waste [G = A3+B3+E+F]	Mass of Useful Products [H = C+D]	E-factor [I = G/H]	PMI [J = I+1]
Run 1	0.498		0.0047	0.1453		3.84	0.0321	4.52	5.0555		0.54
Run 2	0.499		0.0048	0.1521		3.79	0.0318	4.48	5.0555		0.58
Run 3	0.497		0.0051	0.0142		3.88	0.0332	4.43	5.0555		0.62
2. ±	0.0018		0.0004	0.0097		0.09	0.0014	0.08		-	0.08
Aver-age	0.4983		0.0049	0.1466		3.84	0.03237	4.52	5.0555		0.54
3.											

	Input	4.514	0.03629								
	Isolated	3.84	0.03237	0.4983	0.1466	0.0049	0.0005	0.6833	0.6773	1.06	2.06
	Loss	0.674	0.00392								

Table S6: Mass Balance of Methanolysis Reaction

Table S7: Green Metrics of Michael Addition Reaction

Nitrostyrene (g) A	Catalyst (g) B	Michael Product Yield (g) C	Theoretical Yield (g) D	Nitrostyrene Converted (g) [E = 95% of 0.14915]	Nitrostyrene Unconverted (g) [F = A-E]	Total Waste (g) [G = B+F]	E-Factor [H = G/D]	PMI [I = H+1]
0.17898	0.0149	0.237	0.249	0.142	0.037	0.052	0.22	1.22

References:

1. Khiangte V, Lalhmangaihzuala S, Laldinpuii ZT, Nunnemi L, Muthukumaran RB, Vanlaldinpuia K. 2023 Novel dragon fruit peel ash-derived solid catalyst for biodiesel production and PET waste recycling. *Bioresour Technol Rep* 24, 101663. (doi:10.1016/J.BITEB.2023.101663)

2. Laskar IB, Gupta R, Chatterjee S, Vanlalveni C, Rokhum L. 2020 Taming waste: Waste Mangifera indica peel as a sustainable catalyst for biodiesel production at room temperature. *Renew Energy* 161, 207–220. (doi:10.1016/J.RENENE.2020.07.061)

3. Basumatary B, Basumatary S, Das B, Nath B, Kalita P. 2021 Waste Musa paradisiaca plant: An efficient heterogeneous base catalyst for fast production of biodiesel. *J Clean Prod* 305, 127089. (doi:10.1016/J.JCLEPRO.2021.127089)

4. Gohain M, Laskar K, Paul AK, Daimary N, Maharana M, Goswami IK, Hazarika A, Bora U, Deka D. 2020 Carica papaya stem: A source of versatile heterogeneous catalyst for biodiesel production and C–C bond formation. *Renew Energy* 147, 541–555. (doi:10.1016/j.renene.2019.09.016)

5. Guo X, Shi H, Wei X. 2017 Pore properties, inner chemical environment, and microstructure of nano-modified CFA-WBP (class C fly ash-waste brick powder) based geopolymers. *Cem Concr Compos* 79, 53–61. (doi:10.1016/J.CEMCONCOMP.2017.01.007)

6. Thommes M, Kaneko K, Neimark A V., Olivier JP, Rodriguez-Reinoso F, Rouquerol J, Sing KSW. 2015 Physisorption of gases, with special reference to the evaluation of surface area and pore size distribution (IUPAC Technical Report). *Pure and Applied Chemistry* 87, 1051–1069. (doi:10.1515/PAC-2014-1117)

7. Bardestani R, Patience GS, Kaliaguine S. 2019 Experimental methods in chemical engineering: specific surface area and pore size distribution measurements—BET, BJH, and DFT. *Can J Chem Eng* 97, 2781–2791. (doi:10.1002/CJCE.23632)

8. Basumatary B, Brahma S, Nath B, Basumatary SF, Das B, Basumatary S. 2023 Post-harvest waste to value-added materials: Musa champa plant as renewable and highly effective base catalyst for Jatropha curcas oil-based biodiesel production. *Bioresour Technol Rep* 21, 101338. (doi:10.1016/J.BITEB.2023.101338)

9. Changmai B, Sudarsanam P, Rokhum L. 2020 Biodiesel production using a renewable mesoporous solid catalyst. *Ind Crops Prod* 145. (doi:10.1016/j.indcrop.2019.111911)